Metal Organic Frameworks for Hydrogen Purification

Donglai Mao[1], John M Griffin[2,3], Richard Dawson[1], Alasdair Fairhurst[4], Nuno Bimbo[1,5*]

[1]Department of Engineering, Lancaster University, Lancaster LA1 4YW, United Kingdom

[2]Department of Chemistry, Lancaster University, LA1 4YB, United Kingdom

[3]Materials Science Institute, Lancaster University, LA1 4YB, United Kingdom

[4]NanoSUN Limited, Lancaster, LA1 3NX, United Kingdom

[5]Present address: School of Chemistry, University of Southampton, Southampton, SO17 1BJ, United Kingdom

*Corresponding Author: n.bimbo@soton.ac.uk

ABSTRACT: High purity hydrogen is one of the key factors in determining the lifetime of proton exchange membrane (PEM) fuel cells. However, the current industrial processes for producing high purity hydrogen are not only expensive, but also come with low energy efficiencies and productivity. Finding more cost-effective methods of purifying hydrogen is essential for ensuring wider scale deployment of PEM fuel cells. Among various hydrogen purification methods, adsorption in porous materials and membrane technologies are seen as two of the most promising candidates for the current industrial hydrogen purification methods, with metal organic frameworks (MOF) being particularly popular in research over the last decade. Despite many available reviews on MOFs, most focus on synthesis and production, with few reports focused on performance for hydrogen purification. This review describes the working principle and performance parameters of adsorptive separations and membrane materials, and identifies MOFs that have been reported for hydrogen purification. The MOFs are summarized and their performance in separating hydrogen from common impurities (CO_2, N_2, CH_4, CO) is compared systematically. The challenges of commercial application of MOFs for hydrogen purification are discussed.

Highlights:

- Different types of metal organic frameworks that have been reported for H_2 purification are summarised and compared.
- Metal organic frameworks with the highest H_2 permeance value are identified.
- Metal organic frameworks with the highest overall H_2 separation factors against various impurity gases are identified.
- Metal organic frameworks with a good balance of permeance and selectivity have been identified.
- Future research direction of metal organic frameworks for H_2 purification is discussed.

Keywords: Metal Organic Frameworks, MOF, Hydrogen, Purification, ZIF, Zeolitic imidazolate frameworks, Adsorption

Word Count: 7152

1. Introduction

With the fast-growing world population, demand for energy has increased exponentially in the past few decades [1]. Despite the fact that they are inherently limited (see Table 1) [2], fossil fuels still account for 77.2% source of power generation globally (see Figure 1) [3]. In order to meet the energy demand and reduce greenhouse gas emissions, alternative energy sources such as geothermal, hydro, marine, solar, wind, and biomass are being utilized in greater quantities [2, 4]. However, the intermittent generation of electricity from such renewables sources gives rise to many challenges in managing grid demand [5]. To help solve the above issues, hydrogen-based energy system has been suggested by many researchers [6-8]. The system employs hydrogen as an energy carrier to transfer energy from various sources into electricity [9-12]. Hydrogen, one of the most promising vehicles through which a zero-carbon economy may be delivered, is abundant on Earth, does not produce harmful emissions at point of use and can be used to convert chemical to electrical energy efficiently in fuel cells. There are also multiple pathways to produce, store and convert hydrogen energy, allowing for great flexibility in

both mobile and static applications [13-16]. However, it is worth noting that hydrogen is highly flammable and relevant safety measures should be put in place when handling hydrogen. This include installing hydrogen sensors, performing regular gas leakage checking on joints, separating energy management system controls from the operator, etc [17-19]. The system does not only have the advantage of clean emission, the high energy density per unit mass of hydrogen also helps smooth the fluctuations in renewable supply and match these with the inherent variability of market demand [16, 20-22]. In addition, with many countries investing in the development of hydrogen and fuel cells, the market value is expected to reach 11 billion USD by 2025 [16].

Table 1. Global fossil fuel statistics based on proved reserves (Adapted from [2])
*: End dates may shift ahead after new discoveries

Fuels	Total reserves	Production/day	End (date)*
Oil	1.689 Trillion barrels	86.81 Million barrels	2066
Gas	6558 Trillion cubic feet	326 Billion cubic feet	2068
Coal	891.531 Billion tons	21.63 Million tons	2126
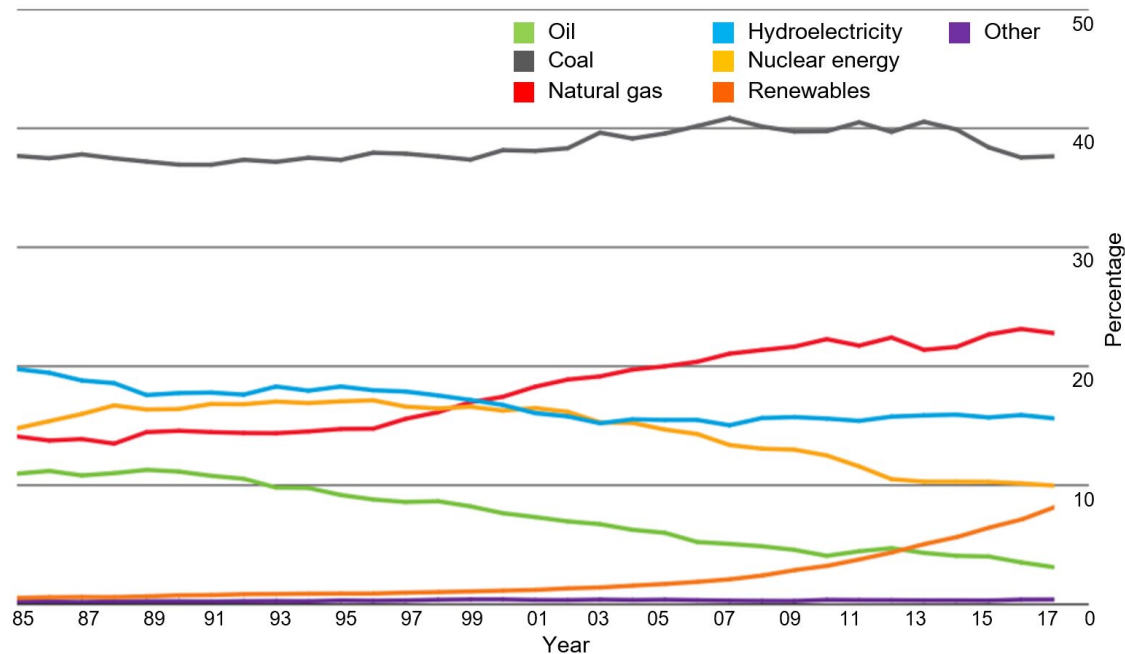
Figure 1. The share of global electricity generation by fuel (Percentage). Taken from [3].

Fuel cells are the most efficient method for converting energy using hydrogen. One of the most promising types of fuel cells is the proton-exchange membrane fuel cell (PEMFC). It has the advantages of fast start-up, high system efficiency (40-50%, compared to 20–35% for the internal combustion engines), and low working temperature, among others. Furthermore, with hydrogen being the primary fuel, it only generates water as a by-product with no harmful pollutants at point of use [13, 14]. However, it has a strict requirement for hydrogen purity, since only 10 ppm CO impurities in hydrogen gas could cause a 28% decrease in the PEMFC performance [15, 23]. Cheng *et al* have reviewed the influence of other contaminants on the performance of PEMFC, which was later summarized by Besancon *et al* in the form of a table (see Table 2) [24, 25]. The hydrogen fuel quality requirement for PEMFC applications in road vehicles has been specified by ISO 14687-2, according to which, high purity hydrogen is required for use in practical applications (see Table 3) [26].
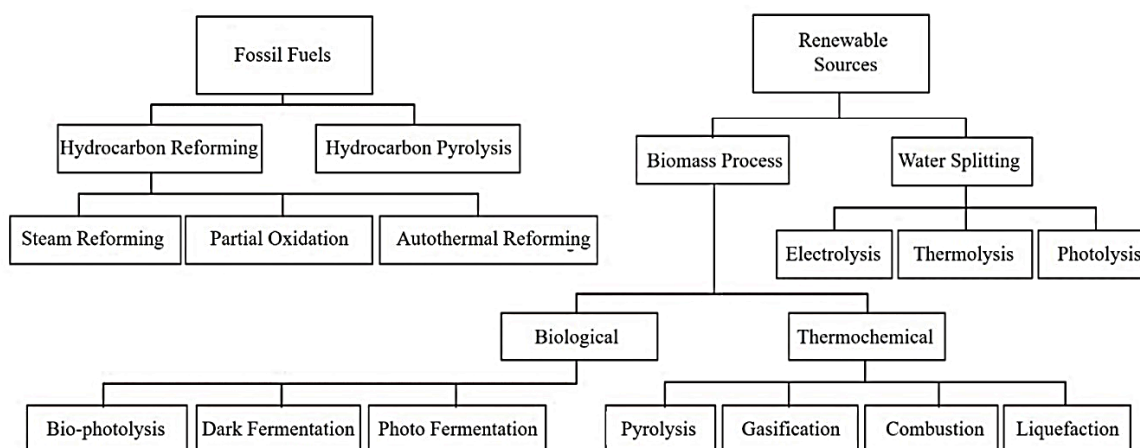
Figure 2. Hydrogen production methods summary. Reprinted from [27]. Copyright (2017), with permission from Elsevier.

Unfortunately, there is a very limited supply of molecular hydrogen on Earth, and they have to be produced from hydrogen-containing compounds such as hydrocarbons and water [28]. According to the source of feedstock (fossil fuels and renewable sources), hydrogen production methods have been categorised and summarised by Nikolaidis *et al* (see Figure 2) [27]. Despite the environmentally friendly appeal of producing hydrogen via methods utilising renewable sources (e.g. bio-photolysis process using biomass in Figure 2), they have the disadvantages of unsolved technological challenges and high costs in comparison to the methods using fossil fuels (e.g. steam reforming process in Figure 2). Therefore, the majority of industrial hydrogen are produced from fossil fuels using the corresponding methods as shown in Figure 2. The hydrogen from these processes can be purified in pressure swing adsorption columns (under temperatures of 21 to 38 °C and pressures of 8- 28 bar [29]), but the resulting product contains impurities such as CO, CO_2, and other minor impurities (i.e. O_2, H_2O, N_2, SO_x, NO_x, sulfur-containing chemicals). Despite these purification steps, low quantities of impurities such as CO can still exist in the product [30-32]. Other hydrogen production methods, such as electrolysis of water and as a by-product of the chlor alkali process, will produce trace amounts of halogens such as chlorine, which without further purification will not meet the strict fuel quality requirements listed in Table 3 [13, 33]. Therefore, further hydrogen purification steps are essential to ensure that the hydrogen quality meets the fuel cell standard [25, 28, 34, 35].

Table 2. The influence of contaminants on PEM fuel cell performance (adapted from [25]).

Contaminant	Impact on fuel cell performance
Carbon monoxide (CO)	Adsorbs to catalyst, degrades performance (reversible)
Sulfur compounds	Adsorbs to catalyst, loss of performance (irreversible)
Ammonia (NH_3)	Degrades membrane ionomer conductivity
Carbon dioxide (CO_2)	Tolerant at 100 ppm – limited CO back shifting
Hydrocarbons	Aromatics, acids, aldehydes, etc. degrade performance
Inert gases (He, Ar, N_2)	Dilution effect only
Particulates	May degrade membrane
Water	Tolerant to >500 ppm
Oxygen	Tolerant to >500 ppm

There are many methods for purifying hydrogen (see Table 4), some of which have been commercialized (e.g. cryogenic separation and pressure swing adsorption), with others still under development [36]. Although PSA and cryogenic processes are the main commercial methods to purify hydrogen, the product purity from both methods is generally not sufficient for fuel cell applications. Further PSA purification cycles can be conducted to improve purity however, this technique comes with a sacrifice in hydrogen recovery [37]. With the high cost associated with the energy requirement for both processes, membrane-based separation technologies have been explored by many researchers. They have the advantages of simple operation, low energy consumption, being environmentally friendly,

amongst others. They are also considered promising methods for delivering high purity hydrogen [38, 39].

Table 3. Fuel quality requirements of hydrogen fuel for PEM fuel cells in road vehicles (Adapted from [26]).

Minimum hydrogen fuel index (mole fraction)	99.97%
Maximum concentration of individual contaminants	
Contaminants	Concentration: mole fraction
Total hydrocarbons (CH_4 basis)	2 ppm
Oxygen	5 ppm
Helium	300 ppm
Total Nitrogen and Argon	100 ppm
Carbon dioxide	2 ppm
Carbon monoxide	0.2 ppm
Total sulphur compounds (H_2S basis)	0.004 ppm
Formaldehyde	0.01 ppm
Formic acid	0.2 ppm
Ammonia	0.1 ppm
Total Halogenated compounds (Halogen ion basis)	0.05 ppm

Among the various types of porous materials for hydrogen purification, metal organic frameworks have received much attention over the last decade. Metal-organic frameworks (MOF) are a new type of porous material composed of metal ions or metal ion clusters, bonded by organic linkers. MOF materials have the advantages of high surface area, tuneable porosity, good selectivity, and flexible structures, which allow for performance adjustment, among other properties [40]. MOFs can also be used in the synthesis of nanostructured membranes, and many reports in this area have been published over the last few years. With the above advantages, extensive research has been carried out to study the material for various applications. According to Yin *et al*, some MOFs have already been applied for delivering gas and storing food commercially [41]. The main characteristics that make MOF popular in gas separation applications are:

(i)   numerous possible combinations of metal centres and organic linkers;
(ii)   potential to adjust pore sizes and inner surface properties through selecting metal centres and organic linkers, as well as using post-synthetic modification method;
(iii)   higher pore volume with lower density [42].

Despite many reviews available for MOF materials, most focus on comparing synthesis methods, modification strategies, and production. Reviews on gas separation performance of the materials also exist, but they are in much shorter supply [42-47]. For example, Zhou *et al* reviewed the performance of MOFs materials in separating various gases. They categorised the MOFs according to the possible adsorption mechanisms and a wide range of gas mixture separation performance were summarised with H_2 purification being a very small part of the paper [43]. Zhu *et al* reviewed synthesis method of MOFs membranes and their applications in separating both gases and liquids. Compared to the previous paper, there is a dedicated section reviewing hydrogen purification in this review. However, it is reported from the perspective of what materials have been reported instead of comparing their performance against each other [46]. Another review on MOFs membranes and their applications in gas separation was reported by Wang *et al*. However, this paper focus on the fabrication methods of MOFs and the issues associated with the corresponding methods [42]. Li summarised the recent progress in production and modification methods of MOFs membranes and the application of MOFs in various areas very comprehensively. Despite covering a wide range of research areas in MOFs, the performance of the materials in purifying H_2 gas was mainly used to prove the effectiveness of different modification methods [47].

This review aims to systematically compare the performance of MOFs in separating hydrogen from common impurities e.g. CO_2, N_2, CH_4, etc., and reviews reports that have used MOFs in both their adsorbent form or in the synthesis of membranes. To our knowledge, the only paper that has extensively reviewed the performance of MOFs in separating H_2 from other impurities during hydrogen production was reported by Azar *et al*. However, this paper only compares the performance of MOFs in separating H_2 from N_2. Other main impurities such as CO, CO_2, and CH_4 were not mentioned [48]. As most of the hydrogen purification reports have focused on membranes, we will first show various separation mechanisms and performance parameters of membrane materials. Different MOFs that have been reported for hydrogen purification will then be compared systematically. Finally, we will summarize the current situation and discuss the future challenges of MOFs in hydrogen purification.

Table 4. Hydrogen purification technologies [36]

Technique	Typical feed gas	Purity (%)	Recovery (%)	Scale of use	Comments
Cryogenic Separation	Petrochemical and refinery off-gases	95-99	90-98	Large scale	Pre-purification step necessary to remove CO_2, H_2S, and water
Polymer Membrane Diffusion	Refinery off-gases and ammonia purge gas	92-98	>85	Small to large	He, CO_2, H_2O may permeate the membrane
Metal Hydride Separation	Ammonia purge gas	99	75-95	Small to medium	Hydrogen adsorption poisoned by O_2, N_2, CO, and S
Solid Polymer Electrolyte cell	Purification of hydrogen produced by thermochemical cycles	99.8	95	Small	Sulfur-containing compounds poison the electrocatalysts
Pressure Swing Adsorption	Any hydrogen rich gas	>99.99	70-90	Large	Relatively low recovery due to hydrogen loss in the purging step.
Catalytic Purification	Hydrogen streams with oxygen impurity	99.999	Up to 99	Small to large	Usually used to upgrade electrolytic hydrogen, organics, Pd-, Hg-, Cd- and S-compounds poison the catalyst. H_2O produced
Palladium Membrane Diffusion	Any hydrogen-containing gas stream	≥ 99.9999	Up to 99	Small to medium	Sulfur and CO-containing compounds and unsaturated hydrocarbon impair permeability.

2. Membrane gas separation mechanisms

Most of the reports that have used MOFs for hydrogen purification have focused on their use as membranes. It is therefore helpful to know the possible gas separation mechanisms of membrane materials so that a better understanding can be developed. A membrane is a thin permeable film that is commonly used for separation and purification [49]. Membranes typically act as selective barriers, allowing only certain molecules to pass through the structure [50]. Several different mechanisms of separation exist, with some common examples being: (1) Poiseuille flow, (2) Knudsen diffusion, (3) molecular sieving, (4) capillary condensation, (5) surface diffusion, (6) solution-diffusion, and (7) facilitated transport. Figure 3 shows the above mechanisms in a schematic form [51, 52]. For membranes which are used to purify hydrogen, the main mechanisms are solution-diffusion and molecular sieving [51]. In the solution-diffusion mechanism, the main influencing factors are solubility and mobility of the gas molecules in the membrane. The most condensable molecules would show better solubility selectivity. At the same time, the smallest molecules tend to diffuse more quickly. Whereas in the molecular sieving mechanism, the main influencing factors are the size of the molecules, where the smallest molecules have a much higher diffusion rate. However, for molecules with similar sizes, factors such as sorption level have a strong impact on the diffusion rate [52].

4

Factors that influence the separation results using membranes include the relative size of molecules to be separated when compared to the pore size of the membrane, the solubility of molecules in the membrane, and dissociative diffusion mechanism [53]. In addition, factors such as partial pressure, concentration of target gases, temperature or electrical potential gradient also affect the process, with the partial pressure being the main driving force in practical applications [54].

Poiseuille Flow Knudsen Diffusion Molecular Sieving Capillary Condensation

Surface Diffusion Solution-Diffusion Facilitated Transport
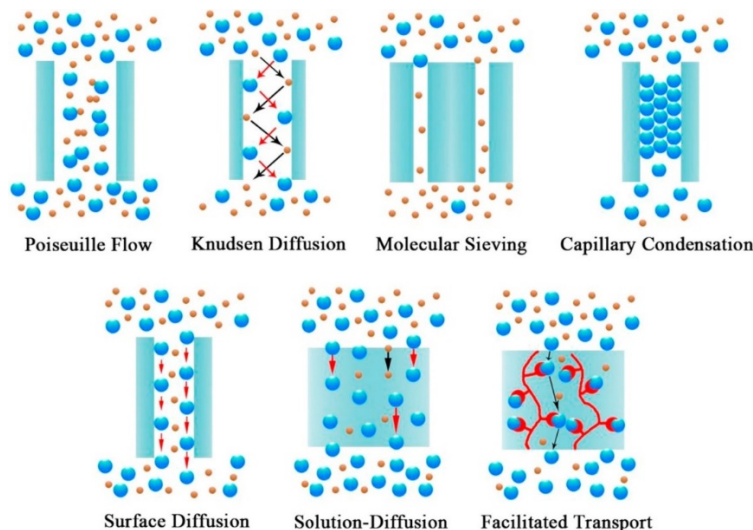
Figure 3. Schematic illustration of gas separation mechanisms in a membrane. Reprinted from [51]. Copyright (2015), with permission from Elsevier.

3. Performance parameters

The main parameters used to assess the performance of a membrane are permeability and selectivity. Permeability indicates the tendency of component flux through the membrane. It equals the product of diffusion coefficient (D) and solubility coefficient (S) of gas in membranes as shown in equation (1).

$$P = D \times S \qquad\qquad\qquad (1)$$

P: permeability, unit: cm^3(STP)cm/cm^2 s cmHg
D: diffusion coefficient, unit: cm^2/s
S: solubility coefficient, unit: cm^3 (STP) /(cm^3 cmHg)

where D is a kinetic parameter and S is a thermodynamic parameter. D is related to the size of the gas molecule, whereas S is associated with the condensability of gas and the interaction between the gas and the membrane. Using materials with higher permeability would lead to better productivity [51, 55-57].

Selectivity shows the ability of a membrane in separating gases. The ideal selectivity of a membrane separating gas A and gas B is shown in equation (2):

$$\alpha_{A/B} = \frac{P_A}{P_B} = \frac{D_A}{D_B} \times \frac{S_A}{S_B} = \alpha_{A/B}^D \times \alpha_{A/B}^S \qquad\qquad (2)$$

where P_A and P_B are the permeability of gas A and gas B respectively; D_A, D_B, S_A, and S_B are the diffusion and solubility coefficients of A and B in the membrane respectively; $\alpha_{A/B}^D$ ($\frac{D_A}{D_B}$) is the diffusion selectivity representing the molecular size difference of A and B, whereas $\alpha_{A/B}^S$ ($\frac{S_A}{S_B}$) is the solubility selectivity showing the adsorption preferences of one gas over the others. Materials with higher selectivity tend to produce hydrogen with greater purity. However, this may mean lower productivity [51, 55-57]. Factors that influence these two parameters include temperature, pressure, humidity, gas compositions, and others [58, 59].

It is worth noting that permeability and selectivity can be used for direct comparison of membranes. However, when choosing membrane materials for commercial applications, fundamental science of the

corresponding material and the scaling up potential should also be considered, since it varies between different membranes [60].

4. MOFs for hydrogen purification

When applied for gas separations, MOFs have been studied in the form of crystalline powders, pelletized systems, and as membranes. MOF materials that have been reported for hydrogen purification include MOF-5, ZIF-7, ZIF-8, ZIF-90, CuBTC, COF, NH_2-MIL-53, MOF-74, UiO-66, etc. Their performance in hydrogen purification is summarized in Table 7, along with the corresponding references. In this section, the permeance and separation factors of the materials are compared. The comparison of separation factors should be used as a guide only when they are obtained by prediction with computer simulation models. This is because the validation of the corresponding data is much more complex for multicomponent adsorption isotherms. General MOF reviews can be found in references [42, 43, 46, 47].

4.1 MOF with multi-carboxylate groups

Multi-carboxylate ligands, benzene-multicarboxylate in particular, are widely used as organic linkers in MOFs. Some of the most commonly used benzene-multicarboxylate linkers are:

- benzene-1,4-dicarboxylate (BDC)
- benzene-1,3-dicarboxylate (IP, as in isophtalic acid)
- benzene-1,3,5-tricarboxylate (BTC)

More details about the roles of these ligands can be found in reference [61] . Here, we mainly focus on the MOFs with these ligands that have been reported for hydrogen separation. These materials are MOF-5, MIL-53 (Al), NH_2-MIL-53(Al), CuBTC/MIL-100, and CuBTC.

4.1.1 MOF-5

MOF-5 is also known as IRMOF-1(isoreticular metal organic framework) and its molecular formula is $Zn_4O(BDC)_3$. Compared to other MOF materials, there are a limited number of reports using this material for hydrogen purification [62]. When MOF-5 was first reported for hydrogen purification, its separation factors were reported as following Knudsen diffusion with a permeance value of $3.00×10^{-6}$ $mol\, s^{-1}\, m^{-2}\, Pa^{-1}$ [62]. Later, the same research group used a different method and synthesised preferentially-oriented MOF-5 membranes. The newly reported MOF-5 showed a lower permeance value than before ($8.00×10^{-7}$ $mol\, s^{-1}\, m^{-2}\, Pa^{-1}$). The selectivity of the material for various gases (see Table 15) was reported to be consistent with the previous study [63].

Another paper on MOF-5 for hydrogen purification application was reported by Lin *et al* [64]. The permeance of this material is lower than what was reported by Lai *et al* [62]. This is not surprising considering the pore size of the sample is smaller (8 Å) than what was reported by Lai *et al* (15.6 Å) [63]. Despite being higher in value than what was reported earlier, the separation factors of various gases in this report are ideal separation factors. The experimental value of separation factors are unknown. It is therefore difficult to compare the performance of MOF-5 with other reports.

The most recent report using MOF-5 to separate hydrogen from other impurities was published by Kloutse *et al* in 2018, and was based on powder adsorbent materials, with the performance measured using a recirculating volumetric method. This is also one of the few papers reporting the performance of MOFs in separating ternary mixtures (H_2:N_2:CO_2=45%:45%:10% and H_2:CH_4:CO_2=42.5%:15%:42.5%) under different pressures (up to 1000kPa at 297K) instead of binary mixtures. It was found that the order of gas adsorption for MOF-5 is $CO_2 > CH_4 > N_2 > H_2$. In addition, the quantity of gas adsorption rises with pressure. Similar results are seen with CuBTC, tested as part of the same study. It is worth noting that azeotropic behaviour was observed for N_2 and CO_2 in H_2-N_2-CO_2 gas mixture with both MOFs, that is, their selectivities changed with composition. This was connected to a high deviation in separation factors when comparing the results from ternary and equivalent binary mixtures. The authors suggest this was caused by a competition between CO_2 and N_2 when they were adsorbed by MOFs. However, this was not observed for the H_2-CH_4-CO_2 gas mixtures [65].

4.1.2 MIL-n

One type of carboxylate containing MOF is the MIL-*n* (MIL: Materials Institute Lavoisier) type with trivalent cations. These types of MOFs have topologies that are similar to zeolites. However, they have different surface chemistry, density and pore sizes [61].

Aluminium 1, 4-benzene-dicarboxylate is normally known as MIL-53 (Al). Its framework consists of infinite chains of corner-sharing $AlO_4(OH)_2$ octahedral. It is famous for its exceptional flexibility, which allows for reversible cell volume adjustment. This leads to better interactions between the guest molecules and the framework. Other advantages of the material include high thermal and chemical stability [66]. The MIL-53 type material that showed the best performance in separating hydrogen from other impurity gases is NH_2-MIL-53 reported by Li *et al*. The material had large pore sizes of 7.5 Å, which contributed to its relatively high permeance. With a thickness of 8 μm, the membrane showed permeance of 5.42×10^{-6} mol s^{-1} m^{-2} Pa^{-1} for H_2 and 4.21×10^{-6} mol s^{-1} m^{-2} Pa^{-1} for H_2/CO_2. The ideal separation factors of the material were 32.4 for H_2/CO_2, 27.9 for H_2/N_2, and 27.3 for H_2/CH_4 [67].

Another MIL-*n* type MOF that showed good performance in separating hydrogen from other impurity gases is CuBTC/MIL-100 fabricated by transforming CuBTC into CuBTC/MIL-100. The above process was achieved by immersing CuBTC hollow fibre into $FeCl_3 \cdot 6H_2O$ methanol solution so that the Fe^{3+} ions could substitute less stable Cu^{2+} ions in CuBTC. The achieved membrane was 20 μm thick and showed H_2 permeance of 8.8×10^{-8} mol m^{-2} s^{-1} Pa^{-1}. Despite the low permeance, the membrane showed very high selectivities in hydrogen separation: 77.6 for H_2/CO_2, 217.0 for H_2/N_2 and 335.7 for H_2/CH_4. In addition, the selectivities and permeance increased with higher temperature. At 85°C, the H_2 permeance was 10.5×10^{-8} mol m^{-2} s^{-1} Pa^{-1} with H_2/CO_2 and H_2/N_2 selectivities being 89.0 and 240.5 respectively. The membrane was able to maintain its high performance for over 192 h [68].

4.1.3 CuBTC
Copper benzene-1,3,5-tricarboxylate (CuBTC) is also known as HKUST-1, $Cu_3(BTC)_2$, MOF-199, and Basolite (TM) C300. Different from ZIFs, CuBTC possesses large pores of 9 Å. Apart from ZIF-8, it is the second most frequently reported MOF for hydrogen purification.

The highest permeance of CuBTC (7.05×10^{-5} mol m^{-2} s^{-1} Pa^{-1}) was reported by Li *et al*. CuBTC was growing on polyacrylonitrile (PAN) to form a $Cu_3(BTC)_2$–PAN hollow fiber membrane via a chemical modification process. The membrane was 13 μm in thickness with a H_2/CO_2 separation factor of 7.1 at 20°C [69].

Although most reported CuBTC membranes showed H_2/CO_2 separation factors that were lower than 10, Zhou *et al* reported a CuBTC membrane which showed a H_2/CO_2 (1:1 v/v) separation factor of 13.6 at 40°C. The material was 13 μm thick with H_2/CO_2 (1:1 v/v) and H_2/CH_4 (1:1 v/v) separation factors of 6.8 and 6.19 respectively. Unfortunately, the permeance of the membrane was relatively low (4.10×10^{-8} mol m^{-2} s^{-1} Pa^{-1} for H_2 in a binary gas mixture) compared to other reports [70].

The highest ideal H_2/N_2 separation factor for CuBTC (13.7 at room temperature) was reported by Shah *et al*. The CuBTC membrane was prepared by a rapid thermal deposition process, which was relatively less time consuming than other traditional fabrication methods (i.e. in *situ* and secondary growth). With a thickness of between 20 and 25 μm, the material also showed an ideal H_2/CH_4 separation factor of 8.8. It is also worth noting that the permeance of the membrane (approximately 3.0×10^{-7} mol m^{-2} s^{-1} Pa^{-1}) was poor [71].

The highest reported H_2/CH_4 (1:1 v/v) separation factor for CuBTC is 11.2 measured at 25 °C. The support material for the CuBTC in this report was stainless steel coated with poly(methyl methacrylate) (PMMA) and poly(methacrylic acid) (PMAA). The membrane was approximately 13 μm thick with relatively high permeance of 1.29×10^{-6} mol m^{-2} s^{-1}. One interesting aspect of this membrane was that it showed higher H_2/CH_4 separation factor than H_2/CO_2 (9.24 for 1:1 v/v) and H_2/N_2 (8.91 for 1:1 v/v). This is different from other reported CuBTC, which generally showed the highest separation factor for H_2/CO_2 followed by H_2/N_2 and H_2/CH_4 (see Table 7). This could be attributed to the polymer coatings on the support material [72].

4.1.4 M-MOF-74
M-MOF-74 is known for its flexibility of accommodating various divalent ions. The metal ions can be one type of ions only or a mixture of different ions [73]. Compared to other MOFs, isostructural M-MOF-74 has larger pore sizes (11 Å). This indicates molecular sieving effect is insignificant during gas separation [74]. There are two main types of MOF-74 reported for hydrogen purification: Mg-MOF-74 (also known as $Mg_2(dobdc)$ or CPO-27–Mg) and Ni-MOF-74. This section will discuss the performance of these two materials that have been reported for hydrogen separation.

Herm *et al* (2011) tested single component CO_2 and H_2 adsorption isotherms of three types of MOFs:

(i) High surface area and rigid framework structure: $Zn_4O(BTB)_2$ (MOF-177, BTB^{3-} = 1,3,5-benzenetribenzoate) and $Be_{12}(OH)_{12}(BTB)_4$ (Be-BTB)
(ii) High surface area and flexible framework: $Co(BDP)$ (BDP^{2-} = 1,4-benzenedipyrazolate)
(iii) Surfaces coated with exposed metal cations: $H_3[(Cu_4Cl)_3(BTTri)_8]$ (Cu-BTTri, $BTTri^{3-}$ = 1,3,5-benzenetristriazolate) and $Mg_2(dobdc)$ ($dobdc^{4-}$ = 1,4-dioxido-2,5-benzenedicarboxylate)

Using ideal adsorbed solution theory (IAST), the authors evaluated the H_2/CO_2 selectivity of the above materials for different $H_2:CO_2$ ratios (80:20 for hydrogen purification and 60:40 for precombustion CO_2 capture) under different conditions. The ideal CO_2/H_2 selectivity for 80:20 ($H_2:CO_2$) mixture is shown in Figure 4. Compared to other MOFs, $Mg_2(dobdc)$ showed the highest selectivities followed by Cu-BTTri, which is also from group III. The author suggested that MOFs with exposed metal cation sites tend to have higher H_2/CO_2 selectivities [75].
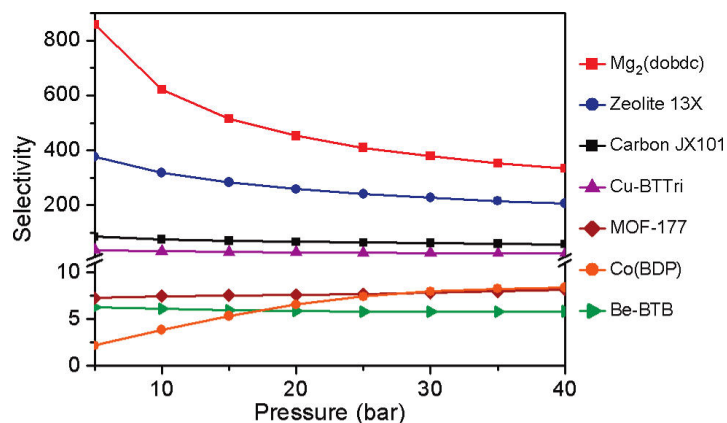
Figure 4. IAST CO_2/H_2 selectivities for a 80:20 H_2/CO_2 mixture at 313 K, as calculated from gas sorption isotherms collected for the metal−organic frameworks MOF-177, Be-BTB, Co(BDP), Cu-BTTri, and $Mg_2(dobdc)$, activated carbon JX101, and zeolite 13X. Reprinted with permission from [75]. Copyright (2011) American Chemical Society.

In 2012, the same group measured CH_4 adsorption isotherms of $Mg_2(dobdc)$ under high pressures. Using the same method, the authors evaluated the selectivity and working capacity of the material for separating gas mixtures of CO_2/CH_4 (1:1 v/v) , CH_4/H_2 (1:1 v/v) and $CO_2/CH_4/H_2$ (1:4:20). The result was compared to 13X zeolite, which showed that the material exhibited 50-75% higher selectivities and almost twice the working capacity of 13X zeolite. In addition, the material regeneration was promising, making it a good candidate for purifying hydrogen [76]. Krishna *et al* reported similar performance for the material [77].

However, Liu *et al* tested the stability of both Mg-MOF-74 and Ni-MOF-74 on CO_2 adsorption and reported that Mg-MOF-74 was less stable and lost considerable amount of CO_2 adsorption capacity in the presence of water vapour. The reported cause was the preferential oxidation of Mg over Ni in the material [78].

Following the above reports, Lee *et al* reported using a two-stage synthesis method to synthesize defect-free Ni-MOF-74 membranes on α-alumina supports. The obtained material showed a high BET surface area of 1318 m^2/g and was able to remain stable at 400°C. With a thickness of 25 μm, the membrane exhibited permeance of 1.27×10^{-5} mol m^{-2} s^{-1} Pa^{-1}. According to the single gas permeation measurements, the ideal H_2/CO_2, H_2/N_2 and H_2/CH_4 separation factors of Ni-MOF-74 membrane were 9.1, 3, and 2.9 respectively. The author compared the results to data from other reports (see Table 5) and concluded that Ni-MOF-74 showed the highest H_2/CO_2 selectivity [79]. This conclusion may require re-evaluation given the advancement of research into more novel MOFs. For example, Wang *et al* modified Mg-MOF-74 membrane via amination of the open Mg sites in the material. The H_2/CO_2 separation factor of the material increased from 10.5 to 28 after the modification. This is much higher than Ni-MOF-74. However, despite being thinner, the permeance of the membrane is significantly lower (2.7×10^{-9} mol m^{-2} s^{-1} Pa^{-1}) than Ni-MOF-74 (10 μm thick) [74].

Table 5. Comparison of gas separation performance of Ni-MOF-74 membrane with other membranes. Adapted from [79].

Membrane	Pore size (nm)	Single gas separation performance selectivity				Permeance (mol m^{-2} s^{-1} Pa^{-1})
		H$_2$/CO$_2$	H$_2$/N$_2$	H$_2$/CH$_4$	CO$_2$/N$_2$	
Polymers	–	–	–	10	–	10^{-12}
MMOF	0.32	–	25[a]	–	1	10^{-9}
ZIF-7	0.30	4~7	–	–	–	10^{-8}
ZIF-8	0.34	4~7	–	–	2~3	10^{-8}
Silicate(1)	0.55	4.4[a]	–	2.1[a]	–	10^{-7}
Silicate(2)	0.55	1.8[a]	3.1[a]	1.8[a]	–	10^{-7}
B-ZSM-5	0.55	2[a]	–	5.8[a]	–	10^{-7}
Cu-BTC(1)	0.9	4.5	4.6	7.8	1	10^{-6}
Cu-BTC(2)	0.9	5.1	3.7	2.9		10^{-7}
Ni-MOF-74	1.58	9.1	3	2.9	3	10^{-6}

[a] 200 °C.

In addition, the Ni-MOF-74 material reported by Al-Naddaf *et al* showed much higher ideal selectivity values than the other reported M-MOF-74 materials for H$_2$ purification. In this report, Ni-MOF-74 was grown on top of zeolites to form a core-shell composite (see Figure 5). The author tested samples with different ratios of Ni-MOF-74 and zeolite. The ideal selectivity values of the samples are shown in Table 6. The author concluded that sample consisted of 95% MOF-74 as the shell and 5% zeolite as the core (Zeo-A@MOF-74-1) showed the best performance compared to zeolite or Ni-MOF-74 in separating hydrogen from corresponding impurities [80].
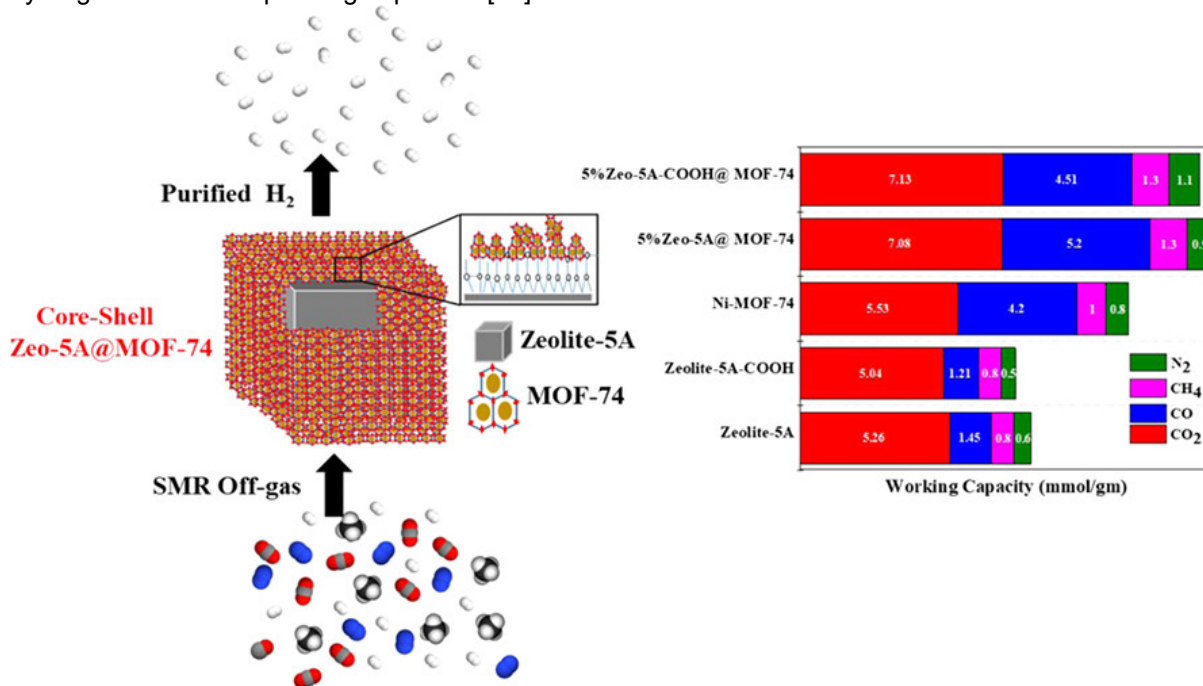
Figure 5. Schematic illustration of core-shell structure of Zeo-A@MOF-74-1 and its gas adsorption capacities. Reprinted with permission from [80]. Copyright (2018) American Chemical Society.

Table 6. Estimated selectivity values for CO$_2$/H$_2$, CO/H$_2$, CH$_4$/H$_2$, and N$_2$/H$_2$. Adapted from [80].

Adsorbent	CO$_2$/H$_2$	CO/H$_2$	CH$_4$/H$_2$	N$_2$/H$_2$
Ni-MOF-74	1084	3903	14	12
zeolite-5A	15 627	796	204	173
zeolite-5A-COOH	2444	65	25	14
Zeo-A@MOF-74-1	8659	24 375	114	45
Zeo-A@MOF-74-2	1984	7039	33	25

Zeo-A@MOF-74-3	1514	5321	29	20
Zeo-B@MOF-74-1	1984	4624	20	13
Zeo-B@MOF-74-2	1329	2219	13	12
Zeo-B@MOF-74-3	860	1695	12	10

4.1.5 UiO-66

The molecular formula of UiO-66 (Universitetet i Oslo) is $Zr_6O_4(OH)_4(bdc)_6$. This material has the advantages of high chemical, thermal and mechanical stabilities. Banu *et al* used Grand canonical Monte Carlo and molecular dynamics simulations to determine the potential of zirconium oxide based MOFs (ehydroxylated UiO-66(Zr), UiO-66(Zr)-Br, UiO67(Zr), and Zr−Cl_2AzoBDC) for purifying hydrogen in steam methane reforming (SMR) off-gas [81]. The results were compared to the performance of a commercial 5A zeolite and activated carbon. It was found that UiO-66(Zr) showed the highest working capacities for CO_2 and CH_4 (pressure range: 1-7 bar) due to its large relative pore volume (see Figure 6). The selectivities of the samples were evaluated using binary mixtures. The H_2/impurity ratio in binary gases was 70/30. It was found that UiO-66(Zr)-Br showed the highest N_2 and CO selectivities and working capacities due to its small and functionalised pores (see Figure 7). According to the breakthrough curve simulations, UiO-66(Zr) and UiO-66(Zr)-Br exhibited longer breakthrough time than the other materials with UiO-66(Zr)-Br showing the longest time. This indicates these two materials would deliver a larger quantity of hydrogen. By comparing various factors, UiO-66(Zr)-Br was suggested as the most promising adsorbent material [81].

Friebe *et al* synthesised UiO-66 membrane with pore sizes of 6 Å on α-Al_2O_3 supports (5 µm thick). The experimentally determined gas permeance is shown in Figure 8. The separation factors for various gas mixtures were H_2/CO_2 (1:1 v/v) = 5.1, H_2/N_2 (1:1 v/v) = 4.7, and H_2/CH_4 (1:1 v/v) = 12.9 [82], although it seemed that the experimentally obtained separation factors are significantly lower than the theoretical separation factors which were reported by Banu *et al* [81]. It is worth noting that the gas mixture content is very different between two reports.
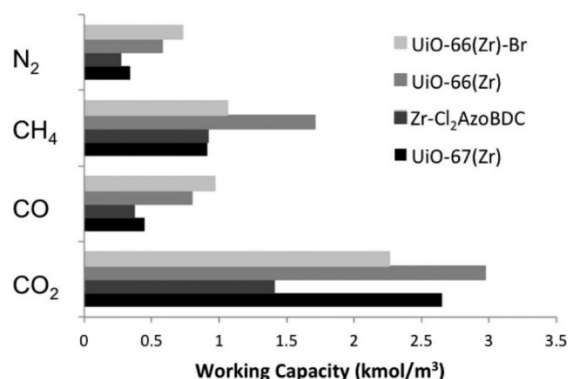
Figure 6. Working capacities from binary-mixture simulations for all impurities for a PSA operating range of 1−7 bar at 298 K. Reprinted with permission from [81]. Copyright (2013) American Chemical Society.
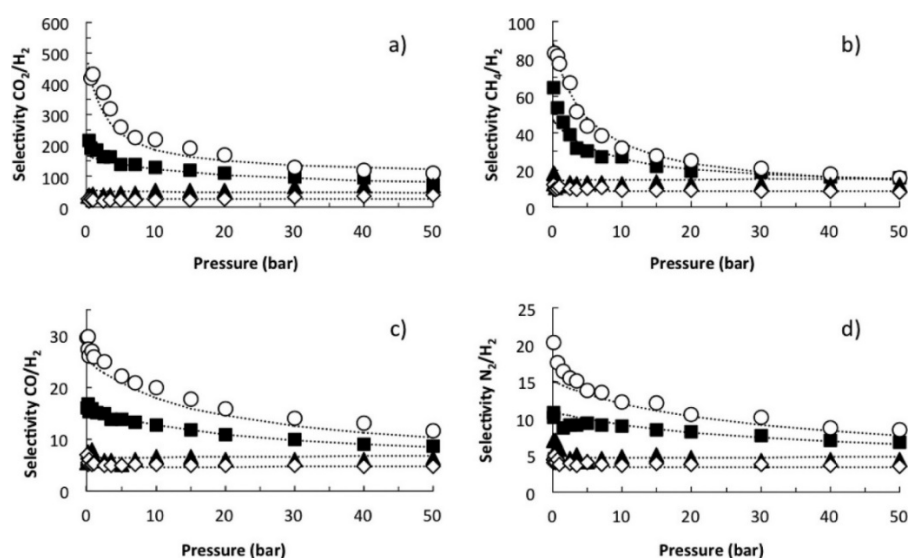
Figure 7. Selectivities from binary-mixture adsorption of (a) CO_2/H_2 30:70, (b) CH_4/H_2 30:70, (c) CO/H_2 30:70, and (d) N_2/H_2 30:70. UiO-67(Zr), solid triangles; Zr−Cl_2AzoBDC, open diamonds; UiO-66(Zr), solid squares; UiO-66(Zr)-Br, open spheres. The dotted lines represent the dual-site Langmuir fitted curves K. Reprinted with permission from [81]. Copyright (2013) American Chemical Society.
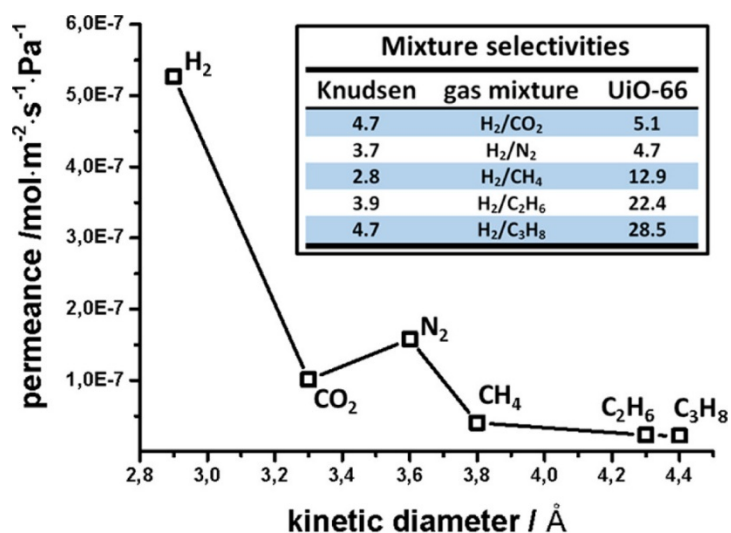
Figure 8. Gas mixture permeances for CO_2, N_2, CH_4, C_2H_6, and C_3H_8, in binary mixtures with H_2 as a function of the kinetic diameter at 25 °C and 1 bar. Inset shows the comparison between the measured mixture separation factors and the corresponding Knudsen values for the binary gas mixtures. Reprinted with permission from [82]. Copyright (2017) American Chemical Society.

4.1.6 Other carboxylate containing MOFs

Other MOF materials that also contain multi-carboxylate include $Zn_2(cam)_2$dabco [83], Zn(BDC)(TED)$_{0.5}$ [84], CAU-1 [85], CAU-10-H [86], etc. Their permeance and selectivities for different gases are in a similar range as the carboxylate containing MFOs mentioned above and shown in table 7. It is worth noting that CAU-10-H, which was tested in a H_2/CH_4 (1:1 v/v) gas mixture at 200°C, showed a selectivity of 74.7. However, the permeance of the material was not very high (1.53×10^{-8} mol m^{-2} s^{-1} Pa^{-1}) and still needs improvement. More details about these materials can be found in the corresponding references.

4.2 Zeolitic imidazolate frameworks (ZIF)

Zeolitic imidazolate frameworks (ZIF) are one type of MOFs with similar topology to zeolites. They consist of transition metal ions (e.g. Co^{2+} and Zn^{2+}) which are coordinated tetrahedrally by imidazole-based (Im) ligands. Each Im ligand connects two metal ions via their nitrogen atom (see Figure 9) [87]. They are one of the most widely studied MOF materials for hydrogen separation. The main types of ZIFs that have been reported for hydrogen separation are ZIF-7, ZIF-8, ZIF-90, ZIF-94, and ZIF-95.
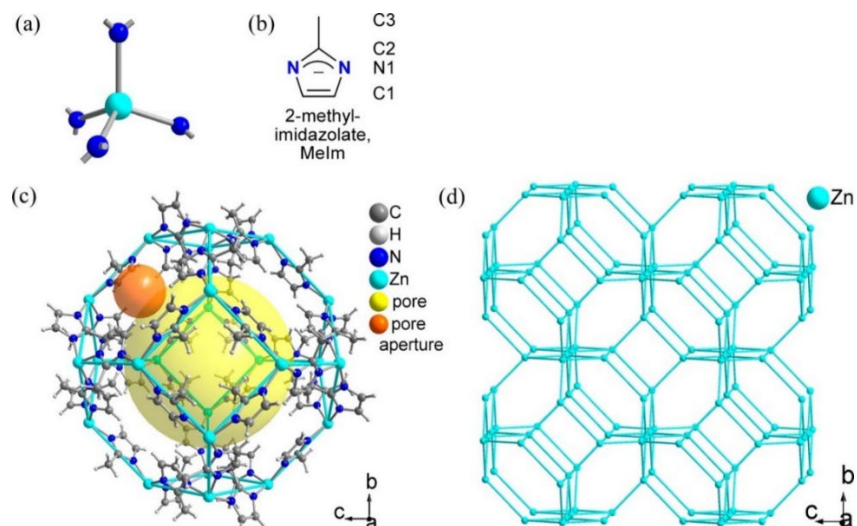
Figure 9. Structure of ZIF-8 (a) Secondary building unit of tetrahedral, nitrogen-coordinated Zn atoms and (b) bridging ligand in ZIF-8. (c) Structure of the ZIF-8 cavity, the yellow sphere with a diameter of 12 Å shows the inner pore of the sodalite cage, and the orange sphere with a diameter of 3.4 Å visualizes the pore aperture window of the SM hexagonal rings (d) MeIm ligands bridge between Zn atoms. Reprinted with permission from [88]. Copyright (2015) American Chemical Society.

4.2.1 ZIF-7

As for ZIF-7, the highest H_2 permeance value reported so far is 2.354×10^{-6} mol s^{-1} m^{-2} Pa^{-1} in the form of an approximately 10 μm thick membrane. The material was prepared using direct crystallization method with PVDF fibre as the support. The ideal separation factors for the corresponding material were 18.4 and 20.3 for H_2/CO_2 and H_2/N_2 respectively [89].

The highest H_2/N_2 (1:1 v/v) separation factor reported for ZIF-7 is 35.1 by Cacho-Bailo *et al* which was obtained experimentally [90]. The membrane was synthesised through direct crystallisation method with a microfluidic system. The ZIF-7 membrane is 2.4±0.4 μm thick on a polysulfone hollow fibre (PSF) support. In addition, the highest experimentally obtained H_2/CH_4 (1:1 v/v) separation factor is also reported in the same paper (34.6). Despite its high selectivity and thin layer, the permeance of the membrane is significantly lower compared to other ZIF-7 materials that have been reported. In addition, its H_2/CO_2 (1:1 v/v) separation factor is 2.4, which is significantly lower than expected [90].

The highest H_2/CO_2 separation factor for ZIF-7 material was 23.2, reported by Li *et al* [91]. The ZIF-7 material in this report was coupled together with reduced graphene oxide (rGO) to form a composite membrane with ZIF-7 existing between the layers of rGO. An *in-situ* method was used to prepare the material on a PVDF fibre support. Unfortunately, in spite of being relatively thin (7 μm thick), this material showed very low permeance (approximately 2×10^{-10} mol s^{-1} m^{-2} Pa^{-1}) compared to other materials [91]. More research is needed to improve both permeance and selectivity of ZIF-7 in hydrogen purification.

4.2.2 ZIF-8

As an important member of MOF family, ZIF-8 is one of the most widely studied MOFs for hydrogen purification. The pore sizes of ZIF-8 (3.4 Å) and hydrophobic behaviour are important characteristics allowing for promising performance in H_2 separation applications [92].

The highest reported H_2 permeance for ZIF-8 is 5.73×10^{-5} mol m^{-2} s^{-1} Pa^{-1} with ZIF-8 being a 2 μm thick membrane at room temperature. The membrane was synthesised using contra-diffusion method on an Al_2O_3 tube substrate. Its H_2/CO_2 and H_2/N_2 separation factors were 15.5 and 17.1 respectively, which are in the range of expected values for ZIF-8 [93].

The highest H_2/CO_2 (1:1 v/v) separation factor for ZIF-8 membrane that has been reported is 34 by Zhang *et al* in 2017. Its H_2/N_2 and H_2/CH_4 separation factors were 20 and 38 respectively. The membrane material was synthesised using a spatially confined contra-diffusion procedure. This involved using polydopamine-wrapped single-walled carbon nanotube (PD/SWCNT) to construct a nanoporous network as an interlayer to control the growth of ZIF-8. The ZIF-8 membrane was 0.55 μm

in thickness with a corresponding H_2 permeance of only 5.75×10^{-7} mol m^{-2} s^{-1} Pa^{-1}. The relatively low permeance could be due to the small pore sizes of the PD/SWCNT interlayer, since they are in the 5-10 nm range. This is much smaller than other substrate materials commonly used for contra-diffusion synthesis where pore diameters are typically greater than 100 nm [94].

The above reasoning is supported by Hou *et al,* who reported a method for fast production of ZIF-8/g-C_3N_4 (graphitic carbon nitride nanosheet) membrane at room temperature [95]. This method also involved combining ZIF-8 membrane with materials of small pore sizes (g-C_3N_4 pore size: 0.31 nm). The membrane was only 0.24 µm thick with a high H_2/CO_2 (1:1 v/v) selectivity of 26. However, the permeance of H_2 at 3.5×10^{-8} mol m^{-2} s^{-1} Pa^{-1}, was a single order lower than values reported by Zhang *et al* [94].

Another example supporting the above point of view is the report from Li *et al*. In this report, the ZIF-8 was also prepared by interfacial contra-diffusion method (see Figure 10). The interlayer material employed in this case was reduced graphene oxide (rGO) [96]. The reported pore size of graphene oxide is approximately 0.11 nm [97], which is even smaller than the above interlayer materials. Not surprisingly, even with a thickness of only 0.15 µm, the obtained material showed only slightly higher H_2 permeance, approximately 6.7×10^{-7} mol m^{-2} s^{-1} Pa^{-1}, than the value in the report from Zhang *et al* [94]. Despite the low permeance, the material showed high separation factors for all three different binary gas mixtures (25.3 for H_2/CO_2, 70.4 for H_2/N_2, 90.7 for H_2/CH_4) [96]. However, it is worth noting that the ratios of gases in the gas mixture for selectivity tests were not clarified in this paper.

The highest H_2/N_2 (1:1 v/v) and H_2/CH_4 (1:1 v/v) separation factors for ZIF-8 membrane were reported to be 90.5 and 139.1 by Huang *et al*. The H_2/CO_2 (1:1 v/v) separation factor of the membrane was 14.9 and lower than the other two gas mixtures. It is also worth pointing out that the selectivity test was carried out at 250 °C [98]. In this report, ZIF-8 was prepared by depositing its precursor solution onto a modified Al_2O_3 disc. After obtaining semi-continuous ZIF-8 crystals, graphene oxide (GO) was coated onto the surface to seal the gaps in between the crystals and to form the targeted ZIF@GO membrane (see Figure 11). The ZIF-8 membrane was 10 µm in thickness with the parts filled by GO being 0.1 µm in thickness. The H_2 permeance of the membrane was 1.45×10^{-7} mol m^{-2} s^{-1} Pa^{-1} and even lower for binary gas mixtures. The highest H_2/N_2 and H_2/CH_4 separation factors obtained from tests at room temperature were reported by Li *et al* [96].
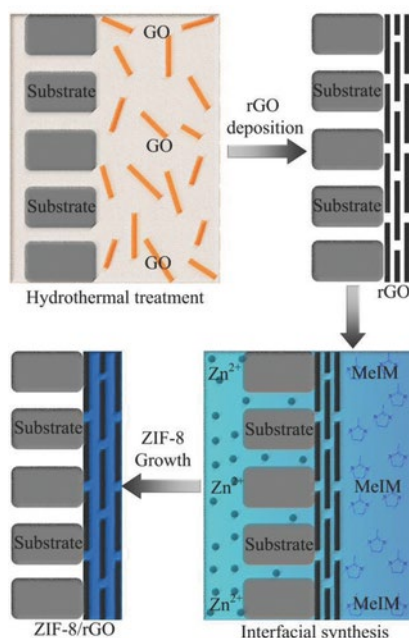
Figure 10. Schematic illustration of interfacial contra-diffusion synthesis of ZIF-8/rGO composite membranes. Reprinted from [96], Copyright (2018), with permission from John Wiley and Sons)

13
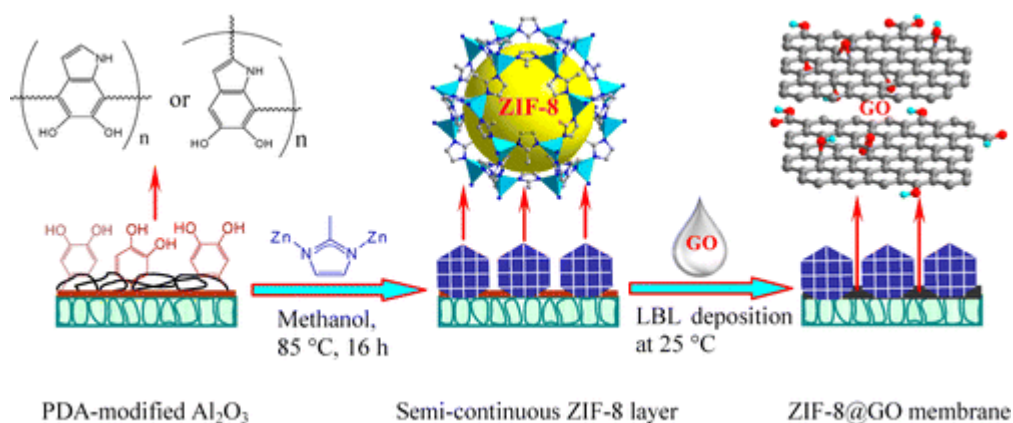
Figure 11. Schematic illustration of synthesis of bicontinuous ZIF-8@GOmembranes through layer-by-layer deposition of graphene oxide onto the semicontinuous ZIF-8 layer. Reprinted with permission from [98], Copyright (2014) American Chemical Society.

4.2.3 ZIF-9

Compared to ZIF-7 and ZIF-8, there is a very limited number of reports on studying ZIF-9 material for hydrogen separation. The highest hydrogen permeance (1.4×10^{-5} mol m^{-2} s^{-1} Pa^{-1}) for ZIF-9 membrane was reported by Zhang *et al* [99]. In this report, ZIF-9 existed in the form of ZIF-9-67 hybrid membrane on α-Al$_2$O$_3$ support. Unfortunately, similar to other membranes with high permeance, the ideal H$_2$/CO$_2$ separation factor was not high, approximately 8.89 at room temperature. This limits the application of the material in hydrogen purification.

The highest ideal H$_2$/CO$_2$ separation factor (40.04) was reported by Huang *et al* in 2015 [100]. ZIF-9 membrane was synthesised via a layer–by-layer deposition method to form a CNT@IL/ZIF-9 hybrid membrane. In this method, ZIF-9 was deposited onto α-Al$_2$O$_3$ support first, before being coved by ionic liquid (IL) functionalised carbon nanotubes (CNTs). This is different from methods in other reports, which used MOF membranes to cover other functional layers instead (see Figure 10 and Figure 12) [96]. The obtained material was 30 μm thick with a pore size of 4.3 Å. The permeance of the material was 5.45×10^{-7} mol m^{-2} s^{-1} Pa^{-1}. The ideal H$_2$/N$_2$ (8.48) and H$_2$/CH$_4$ (10.35) separation factors were also studied in this report. According to the authors best knowledge, there are no other reports on H$_2$/N$_2$ and H$_2$/CH$_4$ separation factors for ZIF-9 membranes. Further research is required to gain a better understanding of the material.
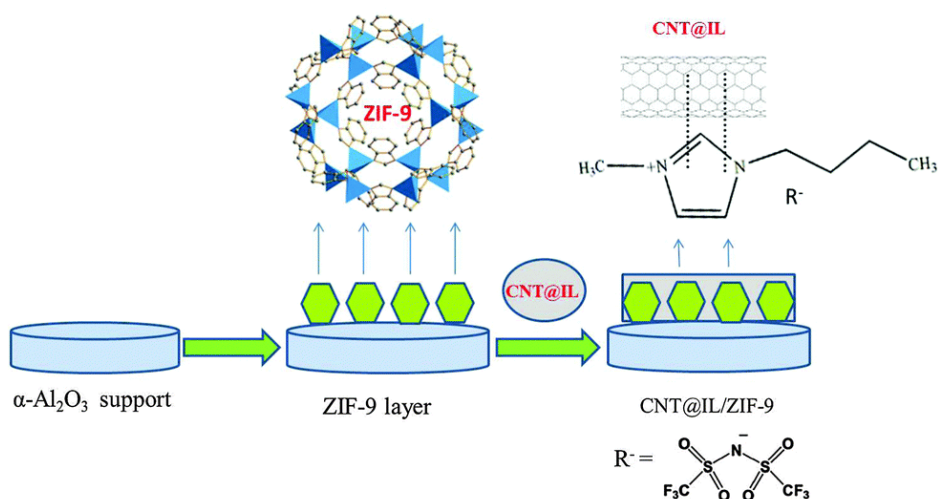
Figure 12. Schematic illustration of preparing CNT@IL/ZIF-9 hybrid membrane via heat treatment of the layer-by-layer deposition of CNT@IL on the ZIF-9 layer with an APTES modified α-Al$_2$O$_3$ support [100]. Republished with permission of The Royal Society of Chemistry, Copyright 2015.

14

4.2.4 ZIF-90

Similar to ZIF-9, the number of papers on investigating ZIF-90 membrane for hydrogen purification is very low with most of them reported by the research group of Huang *et al* [101-105]. The pore size of ZIF-90 is 3.5 Å, similar to ZIF-8. With continuous improvement, the research group managed to fabricate ZIF-90 membrane with a high H_2/CH_4 separation factor (70.5). The corresponding H_2/CO_2 separation factor was 20.1. However, its permeance was lower than expected at 2.85×10^{-7} $mol \, m^{-2} \, s^{-1} \, Pa^{-1}$ for a 20 μm thick membrane, measured at 225 °C [103]. The H_2/N_2 separation factor of ZIF-90 was reported to be 15.8 in earlier reports by the same group. The data was also measured at a high temperature (200°C) [101, 102]. Compared to the best performance that has been reported for ZIF-8, ZIF-90 requires further study to improve performance.

4.2.5 Other ZIFs

Other ZIF materials that have been investigated for hydrogen purification include ZIF-22 [106], ZIF-67 [107], ZIF-78 [108], ZIF-94 [109], ZIF-95 [110], etc the majority of which require further improvements. Among these materials, ZIF-94 showed the highest H_2/CH_4 separation factor (85.6), which was measured at 35 °C. However, the permeance of it (1.6×10^{-8} $mol \, m^{-2} \, s^{-1} \, Pa^{-1}$) was lower than ZIF-90, despite it being only 7.1 μm thick [109]. ZIF-95 showed the highest H_2/CO_2 separation factor (25.7) at room temperature. With the thickness of 30 μm, the material showed permeance of 1.95×10^{-6} $mol \, m^{-2} \, s^{-1} \, Pa^{-1}$ [110]. More details can be found in references 93 to 97.

4.3 M-bim MOFs

Peng *et al* reported an exfoliation method to prepare $Zn_2(benzimidazole)_4$ ($Zn_2(bim)_4$) molecular sieve nanosheets (MSN) from layered MOFs. This involved ball milling $Zn_2(bim)_4$ followed by exfoliation using ultrasonication. With the thickness of 1 nm, the MSN showed a hydrogen gas permeance of up to 9.2×10^{-7} $mol \, m^{-2} \, s^{-1} \, Pa^{-1}$ and H_2/CO_2 (1:1 v/v) separation factor of over 230. In addition, the performance of the material did not deteriorate after testing under varied conditions for over 400 hrs. When combining multiple sheets together through lamellar stacking, the performance of the material was reported to improve further [111]. However, in 2017, the same group used the same method to prepare $Zn_2(bim)_3$ nanosheets with a thickness of 10 nm where a decrease in selectivity was observed. The H_2/CO_2 (1:1 v/v) selectivity of the material was 166 with H_2 permeance of 8×10^{-7} $mol \, m^{-2} \, s^{-1} \, Pa^{-1}$ [112].

Nian *et al* used a vapor phase transformation method (see Figure 13) to synthesise a 57 nm thick $Co_2(bim)_4$ membrane. This method involved coating α-alumina substrate with Co-based gel before heating it in an autoclave. The autoclave contained benzimidazole (bim), which would vaporise during heating process and react with the gel to form $Co_2(bim)_4$. The sample exhibited H_2 permeance of 1.27×10^{-7} $mol \, m^{-2} \, s^{-1} \, Pa^{-1}$ at 30°C. The corresponding H_2/CO_2 (1:1 v/v) , H_2/N_2 (1:1 v/v) , and H_2/CH_4 (1:1 v/v) separation factors were 42.7, 38.4 and 51.3 respectively. It was also pointed out by the author that the H_2/CO_2 separation factor would increase with temperature. At 150°C, the separation factor increased to 63 from 42.7. This was due to higher H_2 permeance and unchanged CO_2 permeance at high temperature [113].
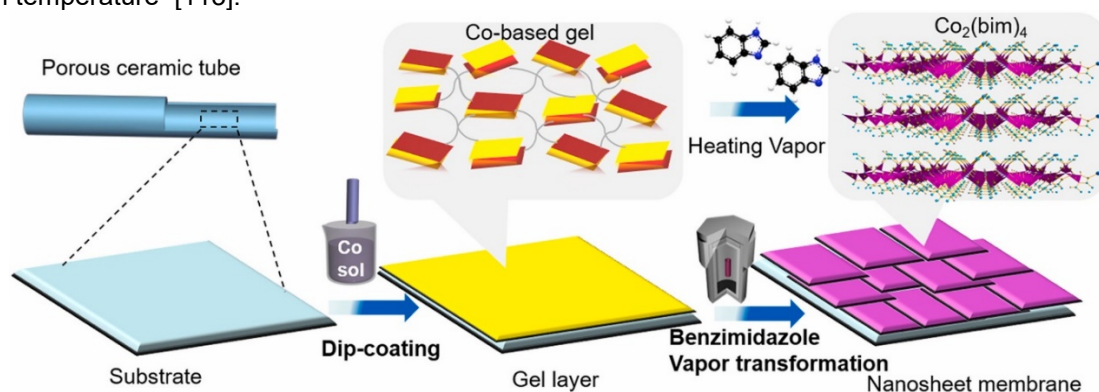
Figure 13. Schematic illustration of $Co_2(bim)_4$ membrane preparation via vapour phase transformation process. Reprinted from [113], Copyright (2018), with permission from Elsevier.

4.4 UTSA-16

K(H$_2$O)$_2$Co$_3$(cit)(Hcit)] (UTSA-16) was first reported by Xiang *et al* for CO$_2$ capture [114, 115]. Using experimentally measured adsorption and diffusion data of various gases (H$_2$, N$_2$, CO, CH$_4$ and CO$_2$) in the material, Agueda *et al* reported the performance for hydrogen purification and recovery in a simulated PSA process. With a rinse step in the PSA cycle, 99.99–99.999% pure hydrogen was generated from the process. The recovery was 93-96% with productivities ranging from 2 to 2.8 mol kg^{-1} h^{-1}. The report also pointed out that the adsorption capacity of UTSA-16 for CO$_2$ was higher than BPL activated carbon but lower than 13X zeolite pellets [116].

Delgado *et al* compared the CO$_2$/H$_2$ selectivities of CuBTC, ZIF-8, and UTSA-16 in a gas mixture of CO$_2$:H$_2$ =60:40 in a simulated PSA process. The result showed that UTSA-16 had the highest CO$_2$/H$_2$ selectivity (423) followed by CuBTC (158) and ZIF-8 (52.4). In addition, when pressure was lower than 5 bar, the sequence of CO$_2$ adsorption capacity was UTSA-16 > CuBTC > ZIF-8. When the pressure is higher than 5 bar, the corresponding sequence became CuBTC> UTSA-16> ZIF-8 [117].

Brea *et al* compared the performance of MOF UTSA-16 and BPL activated carbon in PSA hydrogen purification. The volume ratio of the tested gas mixture is H$_2$: CO$_2$: CO : CH$_4$ = 75.89 : 17.07 : 3.03 : 4.01. The PSA beds studied in the report are (i) layered bed BPL AC/Zeolite 5A and (ii) layered bed UTSA-16/Zeolite 5A. MOF UTSA-16 showed a lower adsorption capacity and recovery than activated carbon. The author attributed the lower performance of UTSA-16 to its higher isotherm curvature for CO$_2$, lower working capacities of CO and CH$_4$, etc. [118].

4.5 COF-MOF

COF (covalent–organic framework)-MOF composite membrane for hydrogen purification was first reported by Fu *et al.* In this report, the MOF materials (Zn$_2$(bdc)$_2$(dabco) and ZIF-8) were grown on chemically modified SiO$_2$ disks which were already covered with COF-300. The thickness of the obtained membranes is shown below:

- [COF-300]-[Zn$_2$(bdc)$_2$(dabco)]: 42 µm for COF-300, and 55 µm for Zn$_2$(bdc)$_2$(dabco)
- [COF-300]-[ZIF-8]: 40 µm for COF-300, and 60 µm for ZIF-8

[COF-300]-[Zn$_2$(bdc)$_2$(dabco)] showed H$_2$ permeance of 4.6×10^{-7} mol m^{-2} s^{-1} Pa^{-1} with H$_2$/CO$_2$ (1:1 v/v) separation factor of 12.6. [COF-300]-[ZIF-8] showed H$_2$ permeance of the 3.6 ×10^{-7} mol m^{-2} s^{-1} Pa^{-1} with H$_2$/CO$_2$ (1:1 v/v) separation factor of 17.2 [119].

Saikat *et al* grew UiO-66 on SiO$_2$ disks first followed by growing COF-300 on top of UiO-66. In the [COF-300]-[UiO-66] composite membrane, COF-300 was 60 µm thick and UiO-66 was 40 µm thick. This material showed a higher H$_2$/CO$_2$ (1:1 v/v) separation factor (17.2) than the above two materials. The permeance of the sample (3.8×10^{-7} mol m^{-2} s^{-1} Pa^{-1}) was, however, lower than the other two materials [120].

4.6 MOFs tested for CO adsorption

Most MOF materials reported for hydrogen purification focus on impurities such as CO$_2$, N$_2$, CH$_4$, and other hydrocarbons. A limited number of papers reported the performance of MOFs in removing CO from hydrogen. These papers are summarized below.

Fischer *et al* used Monte Carlo simulations to compare the CO/H$_2$ selectivity and working capacity of five different materials (zeolite: silicalite; MOFs: Mg-formate, Zn(dtp), Cu$_3$(BTC)$_2$; porous molecular crystal: cucurbit[6]uril). Despite Cu$_3$(BTC)$_2$ exhibited the highest working capacity, it also showed the lowest selectivity (lower than BPL activated carbon) caused by its large pores. However, all the other materials showed higher selectivity than BPL activated carbon whose Henry's law selectivity is α = 12.8. It was highlighted that Mg-formate maintained a high selectivity of α > 30 under all evaluated pressures. The authors concluded that materials with narrow channels showed the best performance in purifying hydrogen due to maximized dispersive interactions. In addition, polar materials have stronger electrostatic interactions with CO, which are preferred in CO/H$_2$ separation [121].

After obtaining single gas adsorption isotherm data, Wu *et al* used IAST to evaluate the selectivities of a *rht*-type metal–organic framework [Cu$_3$(TDPAT)(H$_2$O)$_3$]·10H$_2$O·5DMA (Cu-TDPAT). The gas mixtures investigated in this report were CO$_2$/CO/CH$_4$/H$_2$, CO$_2$/H$_2$, CH$_4$/H$_2$, and CO$_2$/CH$_4$ at pressures up to 70 bar. By comparing the results with other materials (Mg-MOF-74, MIL-101, LTA-5A, and NaX), it was found that the CO$_2$/H$_2$ selectivity of Cu-TDPAT was better than MIL-101, but lower than the others (see

Figure 14). However, the productivity of Cu-TDPAT was higher than more commonly used NaX zeolite when pressures were higher than 20 bar (see Figure 15) [122].
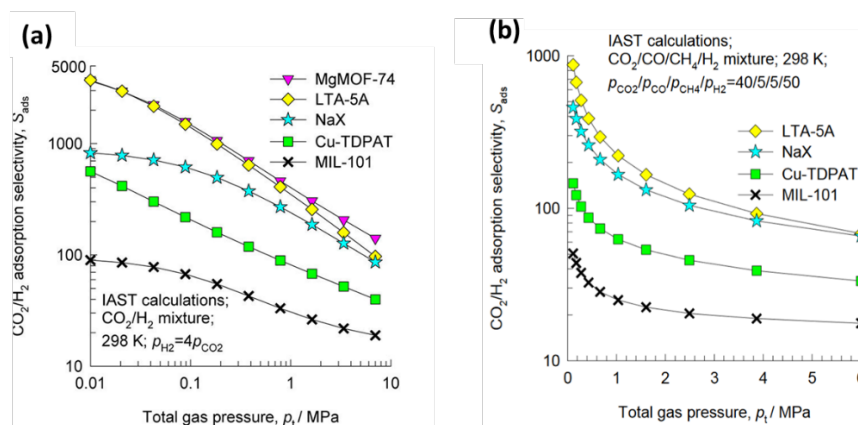
Figure 14. IAST calculations for CO$_2$/H$_2$ selectivity (a) CO$_2$/H$_2$ = 20/80, (b) CO$_2$/CO/CH$_4$/H$_2$ = 40/5/5/50. Reprinted with permission from [122]**, Copyright (2012) American Chemical Society.**

Yin *et al* incorporated ZIF-8 based membrane into a membrane reactor to improve the CO conversion efficiency and the H$_2$ purity in low-temperature water gas shift reactions. According to their single gas permeation tests at room temperature, the 1 μm thick ZIF-8 membrane showed H$_2$, CO and CO$_2$ permeances of 9.2×10^{-7} mol m^{-2} s^{-1} Pa^{-1}, 1.5×10^{-7} mol m^{-2} s^{-1} Pa^{-1}, and 2.3×10^{-7} mol m^{-2} s^{-1} Pa^{-1} respectively. Therefore, the corresponding ideal H$_2$/CO and H$_2$/CO$_2$ separation factors were 6.13 and 4.00. Apart from single gas tests, the group also tested gas separation performance of the membrane for mixed gases (H$_2$: CO: CO$_2$=2:1:1). The resulting permeances of different gases were 6.2×10^{-7} mol m^{-2} s^{-1} Pa^{-1} (H$_2$), 1.2×10^{-7} mol m^{-2} s^{-1} Pa^{-1} (CO), and 1.8×10^{-7} mol m^{-2} s^{-1} Pa^{-1} (CO$_2$). The obtained H$_2$/CO and H$_2$/CO$_2$ separation factors were 4.92 and 3.18 respectively [123].
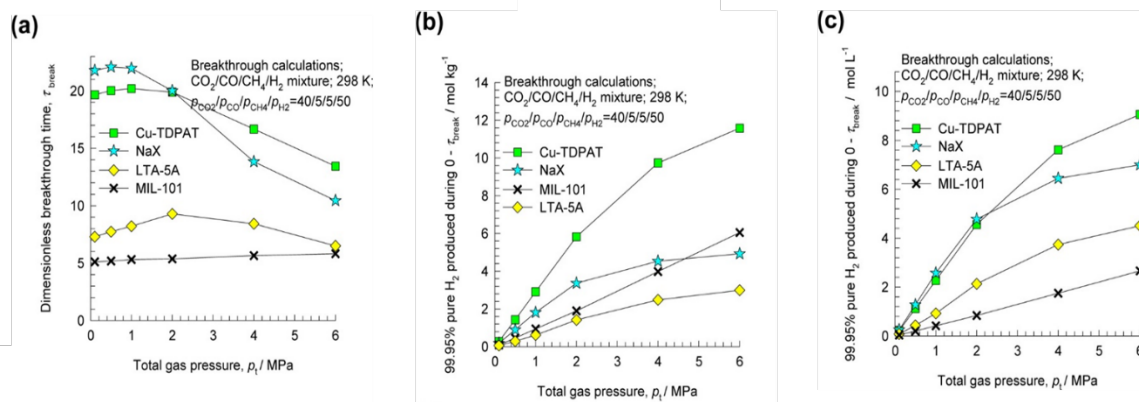
Figure 15. Influence of the total operating pressure on (a) dimensionless breakthrough times and the number of moles of 99.95%+ pure H$_2$ produced (b) per kg of adsorbent material and (c) per L of adsorbent material during the time interval 0−τ$_{break}$. The breakthrough times, τ$_{break}$, correspond to those when the outlet gas contains 500 ppm (CO$_2$ + CO + CH$_4$). Reprinted with permission from [122]**, Copyright (2012) American Chemical Society.**

4.7 Other MOFs

Other MOF materials that have been reported for hydrogen separation (i.e. Zn$_2$(cam)$_2$dabco [83], Cu(hfipbb)(H$_2$hfipbb)$_{0.5}$ [124] , Cu$_2$(bza)$_4$(pyz) [125] , Ni-(4-pyridylcarboxylate)$_2$ [126]) can be found in the references. Ni-(4-pyridylcarboxylate)$_2$ is highlighted here due to its high CO$_2$/H$_2$ selectivities.

Nandi *et al* synthesised a single–ligand Ni-(4-pyridylcarboxylate)$_2$ (Ni-4PyC) MOF material which had ultra-micro porosities of 3.5 and 4.8 Å and a surface area of 945 m^2/g. At 10 bar, 40°C, the material showed CO$_2$/H$_2$ selectivities of 285 for CO$_2$:H$_2$ = 20:80 gas mixture and 230 for CO$_2$:H$_2$ = 40:60 gas mixture. The working capacity of the material was found to be 3.95 mmol/g. In addition, Ni-4PyC was able to remain stable after steam treatment of 160 hrs and presentation under pressure of 70 bar for 24

hrs. Its resistance to humidity during adsorption also made it a very attractive candidate for hydrogen purification [126].

5. Conclusion and outlook

In this review, we have summarised MOFs materials that have been reported for hydrogen purification with a focus on MOFs separating H_2 from the common impurity gases such as CO_2, CH_4, and N_2. Their performance in separating the above impurity gases have been compared systematically to identify high performing materials and to provide reference points for comparing research results for researchers in this area.

- The highest H_2 permeance of MOFs that has been reported so far is CuBTC (7.05×10^{-5} $mol\,m^{-2}\,s^{-1}\,Pa^{-1}$). However, the selectivities of the material are insufficient [69].
- The MOF material showing the highest overall selectivity is CuBTC/MIL-100: 77.6 for H_2/CO_2, 217.0 for H_2/N_2, and 335.7 for H_2/CH_4. Unfortunately, the permeance of the material is not high enough ($8.8 \times 10^{-8}\,mol\,m^{-2}\,s^{-1}\,Pa^{-1}$) [68].
- For commercial applications, MOF materials should possess both high permeance and high selectivities. The most promising material seems to be ZIF-8 reported by Li *et al*. This material exhibited a balance between permeance and selectivity with a permeance of 6.7×10^{-7} mol $m^{-2}\,s^{-1}\,Pa^{-1}$ and separation factors of 25.3 for H_2/CO_2, 70.4 for H_2/N_2, 90.7 for H_2/CH_4 [96]. The ratios of components in the gas mixture were not mentioned in this report nor in the study on CuBTC/MIL-100. Therefore, it is difficult to comment further on the relative performance of the material.

During the review process, research gaps have also been identified and more research could be carried out in the following area in the future:

- There are very few reports on the performance of MOFs in separating hydrogen from CO, which is one of the major impurities in industrial hydrogen and cause more severe damage to fuel cell performance than the other impurity gases. More research should be focused in this area.
- Most reports focus on testing the performance of MOF materials in separating hydrogen in binary gas mixtures. The number of reports of MOF materials separating hydrogen from more than one contaminant gas is very limited. Due to competitive adsorption and desorption of various gases on adsorbents, the separation factors obtained from mixed gas tests can be lower than the values obtained from binary gas tests or single gas tests. Therefore, it is important to focus further research in these areas to provide more reliable data for practical applications.
- The mechanical strength and structural stability of MOFs could be improved, as they are lower than other materials such as zeolites. This is important especially when they are working with feed gases containing aggressive components, under high pressures or made into thin membranes for hydrogen purification.
- The hydrothermal stability of MOFs at high temperatures could be improved if they were to be used to purify hydrogen generated from the water gas shift reaction process as the gas temperature from this process can be very high.
- There is limited understanding of the gas separation mechanisms which occur when using MOF membranes. Developing a better understanding could help identify factors that lead to high performance in MOF materials and help other researchers to tailor their materials to achieve better performance.
- Gas permeance and selectivities of MOFs could be further improved for industrial application.
- The cost of synthesising MOF materials is still very high for commercial applications compared to other traditional materials e.g. the price of a commercial CuBTC is 126 times of 5A zeolites. Although this could be helped by large scale production, MOFs can be very sensitive synthesis conditions. Therefore, it is also important to check the reproducibility of the synthesis method.

Table 7. Summary of MOF materials for H₂ separation (Adapted from Ref [46] with the permission from the Royal Society of Chemistry; Reprinted from Progress in Materials Science, Vol 100, Li W. Metal–organic framework membranes: Production, modification, and applications, Pages 21-63, Copyright (2018), with permission from Elsevier [47])

a:The data was obtained from the single-component permeation. RT: room temperature.

MOF	Substrate	Method	Solvent | Component	Pore size (Å)	Thickness (µm)	Permeance Tem (°C)	Gas pair	Permeance (×10⁻⁸ mol s⁻¹ m⁻² Pa⁻¹) Before	After	Selectivity Before	After	Ref.
MOF-5	α-Al₂O₃ discs	Dip-coating	DMF	15.6	40	RT	H_2/CO_2	80		2.5		[63]
							H_2/N_2			2.7		
							H_2/CH_4			2		
MOF-5	α-Al₂O₃ disks	Coating	EtOH/water	8	14	RT	H_2/CO_2	43		4[a]		[64]
							H_2/N_2			4.1[a]		
MIL-53 (Al)	α-Al₂O₃ disks	Embedding	Al(NO₃)₃·9H₂O	7.3 × 7.7	8	RT	H_2/CO_2	50		4[a]		[127]
							H_2/N_2			2.5[a]		
							H_2/CH_4			2.2[a]		
NH₂-MIL-53(Al)	Porous SiO₂	Deposition	DMF	7.5	15	15-80	H_2/CO_2	200		30.9		[128]
							H_2/N_2			23.9		
							H_2/CH_4			20.7		
NH₂-MIL-53	PVDF fiber	Direct crystallization	DMF	7.5	8	RT	H_2/CO_2	421		32.4		[67]
							H_2/N_2	542[a]		27.9[a]		
							H_2/CH_4			27.3[a]		
MIL-100	PVDF fiber	Embedding	rGO	–	7.5	RT	H_2/CO_2	–	1.3	–	12.5	[91]
CuBTC/MIL-100	PVDF fiber	Substitution	FeCl₃·6H₂O	3.5, 5, 9	20	25	H_2/CO_2	201[a]	7.4	6.4[a]	77.6	[68]
							H_2/N_2			6.2[a]	217.0	
							H_2/CH_4			6.2[a]	335.7	
CuBTC	Copper net	Twin copper source	EtOH/Water	7.8	60	RT	H_2/CO_2	150		6.8		[129]
							H_2/N_2			7		
							H_2/CH_4			5.9		
CuBTC	α-Al₂O₃ disks	Step-by-step deposition	Water	9	25	RT	H_2/CO_2	40-60		4.6		[130]
							H_2/N_2			3.7		
							H_2/CH_4			3		
CuBTC	α-Al₂O₃ tube	Dip-coating	EtOH/Water	9	13	RT	H_2/CO_2	4.1		13.6		[70]
							H_2/N_2			6.8		

MOF	Substrate	Method	Solvent | Component	Pore size (Å)	Thickness (µm)	Permeance Tem (°C)	Gas pair	Permeance (×10⁻⁸ mol s⁻¹ m⁻² Pa⁻¹) Before	After	Selectivity Before	After	Ref.
CuBTC	Porous SiO₂ metal nets	Coating	EtOH/Water	9	–	25	H_2/CO_2 H_2/N_2 H_2/CH_4	129		9.24 8.91 11.2		[72]
CuBTC	Non	Confinement conversion	EtOH/Water	9	5.0	RT	H_2/CO_2 H_2/N_2 H_2/CH_4	158[a]		6.1 5.0 4.0		[131]
CuBTC	PSF flat	Layer by layer	DMF/EtOH/H₂O - DMF/EtOH/H₂O	5-9	25	RT	H_2/CO_2 H_2/C_3H_6	7.9[a]		7.2[a] 5.7[a]		[132]
CuBTC	Al₂O₃ disc	Rapid thermal deposition	DMF	–	20–25	RT	H_2/N_2 H_2/CH_4	30		13.7[a] 8.8[a]		[71]
CuBTC	PAN fiber	Direct crystallization	Water/EtOH	9	13	20	H_2/CO_2	7050.0		7.1		[69]
CuBTC	PVDF fiber	Confinement conversion	EtOH/Water	9	3.0	RT	H_2/CO_2 H_2/N_2 H_2/CH_4	201		8.1 6.5 5.4		[133]
CuBTC	PVDF fiber	Direct crystallization	Water/EtOH	–	43	RT	H_2/CO_2 H_2/N_2	601.2 846.0		7.91 5.87[a]		[134]
CuBTC	PVDF fiber	Embedding	rGO	10	8	RT	H_2/CO_2	–	88	–	10.0	[91]
CuBTC	Al₂O₃ disc	Spray/Layer by layer	EtOH-EtOH	–	0.5	RT	H_2/CO_2	3		8.5		[135]
Ni-MOF-74	α-Al₂O₃ disks	Layer-by-layer	THF+DI	11	25	RT	H_2/CO_2 H_2/N_2 H_2/CH_4	1000		9.1 3.1 2.9		[79]
Mg-MOF-74	Al₂O₃ disc	Grafting	EDA	11	10	25	H_2/CO_2	12	8.2	10.5	28	[74]
UiO-66	α-Al₂O₃	Hydrothermal	DMF	6	5	RT	H_2/CO_2 H_2/N_2 H_2/CH_4	53		5.1 4.7 12.9		[82]
Zn(BDC)(TED)₀.₅	α-Al₂O₃ disk	Direct crystallization	EtOH	7.5	25	RT	H_2/CO_2	270		12.1		[84]

MOF	Substrate	Method	Solvent | Component	Pore size (Å)	Thickness (µm)	Permeance Tem (°C)	Gas pair	Permeance (×10^{-8} mol s^{-1} m^{-2} Pa^{-1})		Selectivity		Ref.
								Before	After	Before	After	
CAU-1	α-Al$_2$O$_3$ tube	Solvothermal reaction	Water/EtOH	3.8	4	RT	H$_2$/CO$_2$ H$_2$/N$_2$ H$_2$/CH$_4$	10		12.3 10.33 10.4		[85]
CAU-10-H	α-Al$_2$O$_3$disc	Solvothermal reaction	Water	–	6	200	H$_2$/CO$_2$ H$_2$/CH$_4$ H$_2$/H$_2$O	1.53		11.1 74.7 5.67		[86]
ZIF-7	α-Al$_2$O$_3$ disks	Microwave-assisted seeded growth	DMF	2	1.5	20–200	H$_2$/N$_2$ H$_2$/CH$_4$	8.00 8.00		7.7 5.9		[136]
ZIF-7	α-Al$_2$O$_3$ disks	Microwave-assisted seeded growth	DMF	3	2	220	H$_2$/CO$_2$ H$_2$/N$_2$ H$_2$/CH$_4$	4.55		13.6 18 14		[137]
ZIF-7	PVDF fiber	Direct crystallization	DMF	–	10	RT	H$_2$/CO$_2$ H$_2$/N$_2$	235.4[a]		18.4[a] 20.3[a]		[89]
ZIF-7	PVDF fiber	Direct crystallization	DMF	3	30	RT	H$_2$/CO$_2$ H$_2$/N$_2$	102.2 132.9[a]		15.86 18.3[a]		
ZIF-7	PSF fiber	Microfluidic/Direct crystallization	EtOH	3	2.4±0.4	35	H$_2$/N$_2$ H$_2$/CH$_4$ H$_2$/CO$_2$ CO$_2$/CH$_4$	0.2 0.09		35.1±4.3 34.6±4.0 2.4±0.4 13.5±2.4		[90]
ZIF-7	Al$_2$O$_3$ disc	Electrospray deposition	DMF	3	4.5	25 150	H$_2$/CO$_2$ H$_2$/CO$_2$	46.1 30.5		9.6 18.3		[138]
ZIF-7	PVDF fiber	Embedding	rGO	3	7	RT	H$_2$/CO$_2$	–	0.33	–	23.2	[91]
ZIF-7-8	Al$_2$O$_3$ disc	Pre-substitution	2BIM/MeIM	3.x - 4	2.0	25	H$_2$/CH$_4$ CO$_2$/CH$_4$	16.0 5.0	8.4 4.5	7.6 1.6	11.4 3.4	[139]
ZIF-7	α-Al$_2$O$_3$ disks	Direct crystallization	MeOH-DMF	3	15	RT	H$_2$/CO$_2$	11.1		19		[140]
ZIF-8	TiO$_2$ disks	Direct crystallization	MeOH	3.4	–	RT	H$_2$/CH$_4$	6.70		11.2		[92]

MOF	Substrate	Method	Solvent | Component	Pore size (Å)	Thickness (µm)	Permeance Tem (°C)	Gas pair	Permeance (×10⁻⁸ mol s⁻¹ m⁻² Pa⁻¹) Before	After	Selectivity Before	After	Ref.
ZIF-8	α-Al$_2$O$_3$ tube	Direct crystallization	MeOH	3.4	20	25	H$_2$/N$_2$	20		10.3		[141]
							H$_2$/CH$_4$			10.4		
ZIF-8	α-Al$_2$O$_3$ disks	Direct crystallization	MeOH	3.4	12	25	H$_2$/N$_2$	17		11.6		[142]
							H$_2$/CH$_4$			13		
ZIF-8	Nylon flat	Contra-diffusion	MeOH-MeOH	–	16	20	H$_2$/N$_2$	197.0[a]		4.3[a]		[143]
ZIF-8	YSZ fiber	Direct crystallization	Water	–	2.0	22	H$_2$/CH$_4$	139		10		[144]
ZIF-8	Al$_2$O$_3$ tube	Contra-diffusion	MeOH-MeOH	–	2.0	RT	H$_2$/CO$_2$ H$_2$/N$_2$	5730[a]		15.5[a] 17.1[a]		[93]
ZIF-8	Porous SiO$_2$	Electrospinning coating	Methanol	3.4	–	25	H$_2$/CO$_2$ H$_2$/N$_2$ H$_2$/CH$_4$	30		7.3 4.9 4.8		[145]
ZIF-8	Nylon flat	Contra-diffusion	Water-Water	–	2.5	20	H$_2$/N$_2$	113[a]		4.6[a]		[146]
ZIF-8	Al$_2$O$_3$ fiber	Microfluidic/Direct crystallization	Water	–	2.0	RT	H$_2$/CO$_2$ H$_2$/N$_2$ H$_2$/CH$_4$	43.2[a]		3.3 11.1 12.1		[147]
ZIF-8	Al$_2$O$_3$ tube	Confinement conversion-Direct crystallization	MeOH-MeOH	–	8.0	25	H$_2$/N$_2$	20.8[a]		10.3[a]		[148]
							H$_2$/CH$_4$			10.4[a]		
ZIF-8	PVDF fiber	Direct crystallization	MeOH	–	50	RT	H$_2$/CO$_2$ H$_2$/N$_2$	201.4[a]		16.3[a] 18.1[a]		[89]
ZIF-8	Al$_2$O$_3$ disc	Layer by layer assembly	MeOH-MeOH	–	1.6	35	H$_2$/CO$_2$ H$_2$/N$_2$ H$_2$/CH$_4$	1.9[a]		5[a] 11[a] 12[a]		[149]
ZIF-8	Al$_2$O$_3$ disc	Confinement conversion/Direct crystallization	MeOH	3.4	20	RT	H$_2$/CO$_2$ H$_2$/N$_2$ H$_2$/CH$_4$	14		4.2 10.0 12.5		[150]
ZIF-8	Al$_2$O$_3$ tube	Confinement conversion-Direct crystallization	MeOH-MeOH	–	6.0	30	H$_2$/CO$_2$ H$_2$/N$_2$ H$_2$/CH$_4$	15.8 16.9 16.7		4.6 8.2 9.8		[151]

MOF	Substrate	Method	Solvent | Component	Pore size (Å)	Thickness (µm)	Permeance Tem (°C)	Gas pair	Permeance ($\times10^{-8}$ mol s^{-1} m^{-2} Pa^{-1}) Before	After	Selectivity Before	After	Ref.
ZIF-8	AAO	Confinement conversion-Direct crystallization	EtOH/Water-Water	3.4	2.5	RT	H_2/CO_2 H_2/N_2 H_2/CH_4	471[a]		3.6[a] 12.5[a] 9.8[a]		[152]
ZIF-8	Al$_2$O$_3$ disc	Embedding	GO	3.4	20	250	H_2/CO_2 H_2/N_2 H_2/CH_4	–	12.7 13.4 12.9	–	14.9 90.5 139.1	[98]
ZIF-8	PES fiber	Direct crystallization	MeOH	4-4.2	20	20	H_2/CO_2 H_2/O_2 H_2/N_2	9.1 9.2 9.3		5.0 6.9 20.4		[153]
ZIF-8	PVDF fiber	Direct crystallization	MeOH	–	40	RT	H_2/CO_2 H_2/N_2	190.3 244.3[a]		12.42 14.3[a]		[134]
ZIF-8	PSF fiber	Microfluidic/Direct crystallization	MeOH	3.4	3.6	35	H_2/N_2 H_2/CH_4	0.5		18.3 17.2		[90]
ZIF-8	Al$_2$O$_3$ tube	Confinement conversion	MeOH	3.4	15–20	100	H_2/CO_2 H_2/CH_4	5–10[a]		7.8[a] 12.5[a]		[154]
ZIF-8	Al$_2$O$_3$ disc	Confinement conversion	DMF/Water	–	0.33	30	H_2/CO_2 H_2/N_2 H_2/CH_4	1.4[a]		7.5[a] 23.2[a] 83.1		[155]
ZIF-8/LDH	Al$_2$O$_3$ disc	Confinement conversion	MeOH	–	1.1/1.3	90	H_2/CH_4 H_2/N_2	4.1[a]		54.1 16.8		[156]
ZIF-8	AAO	Confinement conversion-Direct crystallization	EtOH/Water-EtOH/Water	3.4	2.0	RT	H_2/N_2 H_2/CH_4	768[a]		9.5 14.3		[157]
ZIF-8	AAO	Embedding	GO	3.4	0.1	25	H_2/N_2 H_2/CH_4	–	5.46[a]	–	11.1[a] 11.2[a]	[158]
ZIF-8	AAO	Embedding	PDA-CNT	3.4	0.2	RT	H_2/CO_2 H_2/N_2 H_2/CH_4	–	2870[a]	–	14 18 35	[159]
ZIF-8	PVDF fiber	Embedding	rGO	3.4	7	RT	H_2/CO_2	–	0.7	–	18.8	[91]
ZIF-8	P84 fiber	Annealing	Non	3.4	1.3	35	H_2/CH_4 CO_2/CH_4	0.39 0.1	0.33 0.067	32.4 10.5	65 19.6	[160]
						100	H_2/CH_4	–	1.0	–	101.3	

MOF	Substrate	Method	Solvent | Component	Pore size (Å)	Thickness (µm)	Permeance Tem (°C)	Gas pair	Permeance (×10^{-8} mol s^{-1} m^{-2} Pa^{-1}) Before	After	Selectivity Before	After	Ref.
ZIF-8	PVDF fiber	Direct crystallization	Water	–	1	–	H_2/CO_2 H_2/O_2 H_2/N_2 H_2/CH_4	2010[a]		7.1[a] 8.2[a] 8.2[a] 9.1[a]		[161]
ZIF-8	Al$_2$O$_3$ disc	Spin Coating/Layer by layer assembly	MeOH-MeOH	–	3.0	35	H_2/CO_2	–		4.6		[162]
ZIF-8	Al$_2$O$_3$-ZnO fiber	Confinement conversion-Direct crystallization	MeOH-MeOH	3.4	5–6	RT	H_2/N_2 H_2/CH_4	18.1[a]		10.4[a] 11.7[a]		[163]
ZIF-8	BPPO flat	Contra-diffusion	Water-Water	4.0-4.2	2	RT	H_2/CO_2 H_2/N_2 H_2/CH_4	61[a]		5.5[a] 9.2[a] 10.2[a]		[164]
ZIF-8	AAO	Embedding	Porous-GO	–	0.43	25	H_2/N_2 H_2/CH_4	–	117.6[a]	–	10.0[a] 10.4[a]	[165]
ZIF-8	PVDF fiber	Vapor deposition	Non	12	0.087	RT	H_2/O_2 H_2/N_2 H_2/CH_4	1190[a]		14.1[a] 22.4[a] 27.3[a]		[166]
ZIF-8	Non	Embedding	PDA/SWCNT	3.4	0.55	25	H_2/CO_2 H_2/N_2 H_2/CH_4	–	57.5 63.1[a] 63.1[a]	–	34 20[a] 38[a]	[94]
ZIF-8	AAO	Direct crystallization	Water	3.4	0.5	25	H_2/CO_2 H_2/N_2 H_2/CH_4	830[a]		7.3 15.5 16.2		[167]
ZIF-8	AAO	Embedding	g-C$_3$N$_4$	3.4	0.24	RT	H_2/CO_2	–	3.5	–	26	[95]
ZIF-8	PVDF fiber	Embedding	rGO	3.4	0.15	RT	H_2/CO_2 H_2/N_2 H_2/CH_4	–	66.7 66.0 63.7	–	25.3 70.4 90.7	[96]
ZIF-8	α-Al$_2$O$_3$ disks	Layer by layer assembly	Water-MeOH | Cu/Zn/Al$_2$O$_3$	3.4	1	RT	H_2/CO_2 H_2/CO	62/18 62/12		3.18 4.92		[123]
ZIF-9-67	Al$_2$O$_3$ disc	Pre-substitution	BIM/MeIM	–	30	RT	H_2/CO_2	–	1405	–	8.89	[99]
ZIF-9	Al$_2$O$_3$ disc	Occupation/Coating	CNT/[BMIM][Tf2N]	4.3	30	25	H_2/CO_2 H_2/N_2 H_2/CH_4	710.6[a]	54.5[a]	8.42[a] 2.34[a] 2.86[a]	40.04[a] 8.48[a] 10.35[a]	[100]

MOF	Substrate	Method	Solvent | Component	Pore size (Å)	Thickness (µm)	Permeance Tem (°C)	Gas pair	Permeance ($\times 10^{-8}$ mol s^{-1} m^{-2} Pa^{-1}) Before	After	Selectivity Before	After	Ref.
ZIF-9	P84 fiber	Heteroepitaxial growth	ZIF-8	3	0.9/1.1	150	H_2/CO_2	7.2	8.4	8.0	9.6	[168]
ZIF-9	P84 fiber	Heteroepitaxial growth	ZIF-67	3	1.0/1.1	150	H_2/CO_2	7.2	5.3	8.0	9.0	[168]
ZIF-22	TiO$_2$ disks	Grafting	APTES	3	40	50	H_2/CO_2 H_2/N_2 H_2/CH_4	16		7.2 6.4 5.2		[106]
ZIF-67	Al$_2$O$_3$ disc	Heteroepitaxial growth	ZIF-8	–	0.18	RT	H_2/CO_2 H_2/N_2 H_2/CH_4	2.1 3.4 2.2	1.1 2.1 1.7	6.5 8.9 5.5	13.2 9.3 11.1	[107]
ZIF-78	Porous ZnO	Grafting	DMF	3.8	25	RT	H_2/CO_2 H_2/N_2 H_2/CH_4	10		9.5 5.7 6.4		[108]
ZIF-90	α-Al$_2$O$_3$ disks	Grafting	Ethanolamine	3.5	20	200	H_2/CO_2 H_2/N_2 H_2/CH_4	23.7 24.8 25.1	20.2 21.4 19.4	7.3 11.7 15.3	15.3 15.8 18.9	[101, 102]
ZIF-90	Al$_2$O$_3$ disc	Grafting	APTES	3.5	20	225	H_2/CO_2 H_2/CH_4	29.1 29.0	28.2 28.5	7.2 15.4	20.1 70.5	[103, 105]
ZIF-90	Torlon fiber	Direct crystallization	MeOH	3.5	5	35	H_2/CO_2 H_2/N_2	19.4[a]		1.8[a] 6.3[a]		[104]
ZIF-94	P84 fiber	Grafting	Nonylamine	–	7.1	35	H_2/CH_4	0.42	1.6	136	85.6	[109]
ZIF-95	α-Al$_2$O$_3$ disks	Grafting	APTES	3.7	30	RT	H_2/CO_2	195		25.7		[110]
Zn$_2$(bim)$_4$	α-Al$_2$O$_3$	Hot drop coating	DMF/DEA	2.1	0.001	25	H_2/CO_2	76.4 ± 16.4		230 ± 39		[111]
Zn$_2$(bim)$_4$	α-Al$_2$O$_3$	Hot drop coating	DMF/DEA	2.1	0.01	25	H_2/CO_2	80		166		[112]
Co$_2$(bim)$_4$	α-Al$_2$O$_3$	Vapor phase transformation	EGME	-	0.057	30	H_2/CO_2 H_2/N_2 H_2/CH_4	12.7		42.7 38.4 51.3		[113]
[COF-300]-MOF	SiO$_2$ disc	Heteroepitaxial growth	Zn$_2$(bdc)$_2$(dabco)	–	55/42	RT	H_2/CO_2	81	46	6.0	12.6	[119]
[COF-300]-[ZIF-8]	SiO$_2$ disc	Heteroepitaxial growth	ZIF-8	–	58/42	RT	H_2/CO_2	81	36	6.0	13.5	[119]

MOF	Substrate	Method	Solvent | Component	Pore size (Å)	Thickness (µm)	Permeance Tem (°C)	Gas pair	Permeance ($\times 10^{-8}$ mol s^{-1} m^{-2} Pa^{-1})		Selectivity		Ref.
								Before	After	Before	After	
[COF-300]-[UiO-66]	SiO_2	Heteroepitaxial growth	COF-300	10/20	60/40	RT	H_2/CO_2	83	38	9.2	17.2	[120]
Cu(hfipbb)(H$_2$hfipbb)$_{0.5}$	α-Al$_2$O$_3$ disk	Hydrothermal reaction	Water	3.5	20	25-200	H_2/N_2	1.5		22[a]		[124]
							H_2/CO_2			4[a]		
Cu$_2$(bza)$_4$(pyz)	Al$_2$O$_3$ sheet	Embedding	Acetone	2	100	RT	H_2/N_2	0.688		10[a]		[125]
							H_2/CH_4			19[a]		
Zn$_2$(cam)$_2$dabco	Porous ZnO	Hydrothermal reaction	EtOH	3 × 3.5	6	RT	H_2/N_2	2.7		19.1		[83]
							H_2/CH_4			14.7		
Ni$_2$(l-asp)$_2$(bpe)	Nickel mesh	Occupation	bpe	7.9 × 3.3	20-30	25	H_2/CO_2	–	102	–	24.3	[169]
							H_2/N_2		100		12.1	
							H_2/CH_4		100		7.77	

Acknowledgements

References

[1] Miranda LCM, Lima CAS. On the forecasting of the challenging world future scenarios. Technological Forecasting and Social Change. 2011;78:1445-70.

[2] Abas N, Kalair A, Khan N. Review of fossil fuels and future energy technologies. Futures. 2015;69:31-49.

[3] BP. BP Statistical Review of World Energy 67th edition. 2018. p. 1-56.

[4] Ellabban O, Abu-Rub H, Blaabjerg F. Renewable energy resources: Current status, future prospects and their enabling technology. Renewable and Sustainable Energy Reviews. 2014;39:748-64.

[5] Liang X. Emerging Power Quality Challenges Due to Integration of Renewable Energy Sources. IEEE Transactions on Industry Applications. 2017;53:855-66.

[6] Abe JO, Popoola API, Ajenifuja E, Popoola OM. Hydrogen energy, economy and storage: Review and recommendation. International Journal of Hydrogen Energy. 2019;44:15072-86.

[7] Lin R-H, Zhao Y-Y, Wu B-D. Toward a hydrogen society: Hydrogen and smart grid integration. International Journal of Hydrogen Energy. 2020;45:20164-75.

[8] Smoliński A, Howaniec N. Hydrogen energy, electrolyzers and fuel cells – The future of modern energy sector. International Journal of Hydrogen Energy. 2020;45:5607.

[9] Cipriani G, Di Dio V, Genduso F, La Cascia D, Liga R, Miceli R, et al. Perspective on hydrogen energy carrier and its automotive applications. International Journal of Hydrogen Energy. 2014;39:8482-94.

[10] Marchenko OV, Solomin SV. The future energy: Hydrogen versus electricity. International Journal of Hydrogen Energy. 2015;40:3801-5.

[11] Acar C, Dincer I, Naterer GF. Clean hydrogen and power from impure water. Journal of Power Sources. 2016;331:189-97.

[12] Pinsky R, Sabharwall P, Hartvigsen J, O'Brien J. Comparative review of hydrogen production technologies for nuclear hybrid energy systems. Progress in Nuclear Energy. 2020;123:103317.

[13] Korotkikh O, Farrauto R. Selective catalytic oxidation of CO in H_2: fuel cell applications. Catalysis Today. 2000;62:249-54.

[14] Song C. Fuel processing for low-temperature and high-temperature fuel cells: Challenges, and opportunities for sustainable development in the 21st century. Catalysis Today. 2002;77:17-49.

[15] Borup R, Meyers J, Pivovar B, Kim YS, Mukundan R, Garland N, et al. Scientific Aspects of Polymer Electrolyte Fuel Cell Durability and Degradation. Chemical Reviews. 2007;107:3904-51.

[16] More A. Global Hydrogen and Fuel Cells Market 2019 Analysis by Industry-Size, Share, Trends Evaluation, Revenue, Growing-Demand, Regional Analysis & Forecast 2025. 2019.

[17] Mousavi J, Parvini M. Analyzing effective factors on leakage-induced hydrogen fires. Journal of Loss Prevention in the Process Industries. 2016;40:29-42.

[18] Hadef H, Negrou B, Ayuso TG, Djebabra M, Ramadan M. Preliminary hazard identification for risk assessment on a complex system for hydrogen production. International Journal of Hydrogen Energy. 2020;45:11855-65.

[19] Mair GW, Thomas S, Schalau B, Wang B. Safety criteria for the transport of hydrogen in permanently mounted composite pressure vessels. International Journal of Hydrogen Energy. 2020.

[20] Uyar TS, Beşikci D. Integration of hydrogen energy systems into renewable energy systems for better design of 100% renewable energy communities. International Journal of Hydrogen Energy. 2017;42:2453-6.

[21] Hanley ES, Deane JP, Gallachóir BPÓ. The role of hydrogen in low carbon energy futures–A review of existing perspectives. Renewable and Sustainable Energy Reviews. 2018;82:3027-45.

[22] Martin A, Agnoletti M-F, Brangier E. Users in the design of Hydrogen Energy Systems: A systematic review. International Journal of Hydrogen Energy. 2020;45:11889-900.

[23] Yan W-M, Chu H-S, Lu M-X, Weng F-B, Jung G-B, Lee C-Y. Degradation of proton exchange membrane fuel cells due to CO and CO_2 poisoning. Journal of Power Sources. 2009;188:141-7.

[24] Cheng X, Shi Z, Glass N, Zhang L, Zhang J, Song D, et al. A review of PEM hydrogen fuel cell contamination: Impacts, mechanisms, and mitigation. Journal of Power Sources. 2007;165:739-56.

[25] Besancon BM, Hasanov V, Imbault-Lastapis R, Benesch R, Barrio M, Mølnvik MJ. Hydrogen quality from decarbonized fossil fuels to fuel cells. International Journal of Hydrogen Energy. 2009;34:2350-60.

[26] Standardisation IOf. Hydrogen fuel — Product specification Part 2: Proton exchange membrane (PEM) fuel cell applications for road vehicles. Switzerland, 2012.

[27] Nikolaidis P, Poullikkas A. A comparative overview of hydrogen production processes. Renewable and Sustainable Energy Reviews. 2017;67:597-611.

[28] Holladay JD, Hu J, King DL, Wang Y. An overview of hydrogen production technologies. Catalysis Today. 2009;139:244-60.

[29] Sircar S, Golden TC. Purification of Hydrogen by Pressure Swing Adsorption. Separation Science and Technology. 2000;35:667-87.

[30] Veziroglu TN, Zaginaichenko SY, Schur DV, Baranowski B, Shpak AP, Skorokhod VV. Hydrogen Materials Science and Chemistry of Carbon Nanomaterials: Proceedings of the NATO Advanced Research Workshop on Hydrogen Materials Science an Chemistry of Carbon Nanomaterials, Sudak, Crimea, Ukraine, September 14-20, 2003: Springer Science & Business Media; 2006.

[31] Muradov N. Low to near-zero CO_2 production of hydrogen from fossil fuels: Status and perspectives. International Journal of Hydrogen Energy. 2017;42:14058-88.

[32] Abdalla AM, Hossain S, Nisfindy OB, Azad AT, Dawood M, Azad AK. Hydrogen production, storage, transportation and key challenges with applications: A review. Energy Conversion and Management. 2018;165:602-27.

[33] Ehteshami SMM, Chan SH. The role of hydrogen and fuel cells to store renewable energy in the future energy network – potentials and challenges. Energy Policy. 2014;73:103-9.

[34] Gandia LM, Arzamendi G, Dieguez PM. Renewable hydrogen technologies : production, purification, storage, applications and safety: Elsevier Science; 2013.

[35] Voldsund M, Jordal K, Anantharaman R. Hydrogen production with CO_2 capture. International Journal of Hydrogen Energy. 2016;41:4969-92.

[36] Grashoff BGJ, Pilkington CE, Corti CW. The Purification of Hydrogen. 1983:157-69.

[37] Abdeljaoued A, Relvas F, Mendes A, Chahbani MH. Simulation and experimental results of a PSA process for production of hydrogen used in fuel cells. Journal of Environmental Chemical Engineering. 2018;6:338-55.

[38] Barelli L, Bidini G, Gallorini F, Servili S. Hydrogen production through sorption-enhanced steam methane reforming and membrane technology: A review. Energy. 2008;33:554-70.

[39] Cheng YS, Peña MA, Fierro JL, Hui DCW, Yeung KL. Performance of alumina, zeolite, palladium, Pd–Ag alloy membranes for hydrogen separation from Towngas mixture. Journal of Membrane Science. 2002;204:329-40.

[40] Perez EV, Balkus KJ, Ferraris JP, Musselman IH. Mixed-matrix membranes containing MOF-5 for gas separations. Journal of Membrane Science. 2009;328:165-73.

[41] Yin H, Yip ACK. A review on the production and purification of biomass-derived hydrogen using emerging membrane technologies. Catalysts. 2017;7.

[42] Zhang Y, Feng X, Yuan S, Zhou J, Wang B. Challenges and recent advances in MOF–polymer composite membranes for gas separation. Inorganic Chemistry Frontiers. 2016;3:896-909.

[43] Li J-R, Kuppler RJ, Zhou H-C. Selective gas adsorption and separation in metal–organic frameworks. Chemical Society Reviews. 2009;38:1477-504.

[44] Adams R, Carson C, Ward J, Tannenbaum R, Koros W. Metal organic framework mixed matrix membranes for gas separations. Microporous and Mesoporous Materials. 2010;131:13-20.

[45] Dong G, Li H, Chen V. Challenges and opportunities for mixed-matrix membranes for gas separation. Journal of Materials Chemistry A. 2013;1:4610-30.

[46] Qiu S, Xue M, Zhu G. Metal–organic framework membranes: from synthesis to separation application. Chemical Society Reviews. 2014;43:6116-40.

[47] Li W. Metal–organic framework membranes: Production, modification, and applications. Progress in Materials Science. 2019;100:21-63.

[48] Azar ANV, Velioglu S, Keskin S. Large-Scale Computational Screening of Metal Organic Framework (MOF) Membranes and MOF-Based Polymer Membranes for H_2/N_2 Separations. ACS Sustain Chem Eng. 2019;7:9525-36.

[49] Lu GQ, Diniz da Costa JC, Duke M, Giessler S, Socolow R, Williams RH, et al. Inorganic membranes for hydrogen production and purification: A critical review and perspective. J Colloid Interface Sci. 2007;314:589-603.

[50] Drioli E, Barbieri G, Royal Society of C. Membrane engineering for the treatment of gases. Volume 1, Gas-separation problems with membranes Royal Society of Chemistry; 2011.

[51] Li P, Wang Z, Qiao Z, Liu Y, Cao X, Li W, et al. Recent developments in membranes for efficient hydrogen purification. Journal of Membrane Science. 2015;495:130-68.

[52] Koros WJ, Fleming GK. Membrane-based gas separation. Journal of Membrane Science. 1993;83:1-80.

[53] Nenoff TM, Spontak RJ, Aberg CM. Membranes for Hydrogen Purification: An Important Step toward a Hydrogen-Based Economy. MRS Bulletin. 2006;31:735-44.

[54] Tao Z, Yan L, Qiao J, Wang B, Zhang L, Zhang J. A review of advanced proton-conducting materials for hydrogen separation. Progress in Materials Science. 2015;74:1-50.

[55] Ritter JA, Ebner AD. State‐of‐the‐Art Adsorption and Membrane Separation Processes for Hydrogen Production in the Chemical and Petrochemical Industries. Separation Science and Technology. 2007;42:1123-93.

[56] Freeman BD. Basis of Permeability/Selectivity Tradeoff Relations in Polymeric Gas Separation Membranes. Macromolecules. 1999;32:375-80.

[57] Sanders DF, Smith ZP, Guo R, Robeson LM, McGrath JE, Paul DR, et al. Energy-efficient polymeric gas separation membranes for a sustainable future: A review. Polymer. 2013;54:4729-61.

[58] Bernardo P, Drioli E, Golemme G. Membrane Gas Separation: A Review/State of the Art. Industrial & Engineering Chemistry Research. 2009;48:4638-63.

[59] Strathmann HJAj. Membrane separation processes: current relevance and future opportunities. 2001;47:1077-87.

[60] Ockwig NW, Nenoff TM. Membranes for Hydrogen Separation. Chemical Reviews. 2007;107:4078-110.

[61] Janiak C, Vieth JK. MOFs, MILs and more: concepts, properties and applications for porous coordination networks (PCNs). New Journal of Chemistry. 2010;34:2366-88.

[62] Liu Y, Ng Z, Khan EA, Jeong H-K, Ching C-b, Lai Z. Synthesis of continuous MOF-5 membranes on porous α-alumina substrates. Microporous and Mesoporous Materials. 2009;118:296-301.

[63] Yoo Y, Lai Z, Jeong H-K. Fabrication of MOF-5 membranes using microwave-induced rapid seeding and solvothermal secondary growth. Microporous and Mesoporous Materials. 2009;123:100-6.

[64] Zhao Z, Ma X, Li Z, Lin YS. Synthesis, characterization and gas transport properties of MOF-5 membranes. Journal of Membrane Science. 2011;382:82-90.

[65] Kloutse FA, Hourri A, Natarajan S, Benard P, Chahine R. Hydrogen separation by adsorption: Experiments and modelling of H_2-N_2-CO_2 and H_2-CH_4-CO_2 mixtures adsorption on CuBTC and MOF-5. Microporous and Mesoporous Materials. 2018;271:175-85.

[66] Loiseau T, Serre C, Huguenard C, Fink G, Taulelle F, Henry M, et al. A Rationale for the Large Breathing of the Porous Aluminum Terephthalate (MIL-53) Upon Hydration. 2004;10:1373-82.

[67] Li W, Su P, Zhang G, Shen C, Meng Q. Preparation of continuous NH_2–MIL-53 membrane on ammoniated polyvinylidene fluoride hollow fiber for efficient H_2 purification. Journal of Membrane Science. 2015;495:384-91.

[68] Li W, Zhang Y, Zhang C, Meng Q, Xu Z, Su P, et al. Transformation of metal-organic frameworks for molecular sieving membranes. Nature Communications. 2016;7:11315.

[69] Li W, Yang Z, Zhang G, Fan Z, Meng Q, Shen C, et al. Stiff metal–organic framework–polyacrylonitrile hollow fiber composite membranes with high gas permeability. Journal of Materials Chemistry A. 2014;2:2110-8.

[70] Zhou S, Zou X, Sun F, Zhang F, Fan S, Zhao H, et al. Challenging fabrication of hollow ceramic fiber supported $Cu_3(BTC)_2$ membrane for hydrogen separation. Journal of Materials Chemistry. 2012;22:10322-8.

[71] Shah MN, Gonzalez MA, McCarthy MC, Jeong H-K. An Unconventional Rapid Synthesis of High Performance Metal–Organic Framework Membranes. Langmuir. 2013;29:7896-902.

[72] Ben T, Lu C, Pei C, Xu S, Qiu S. Polymer-Supported and Free-Standing Metal–Organic Framework Membrane. 2012;18:10250-3.

[73] Díaz-García M, Mayoral Á, Díaz I, Sánchez-Sánchez M. Nanoscaled M-MOF-74 Materials Prepared at Room Temperature. Crystal Growth & Design. 2014;14:2479-87.

[74] Wang N, Mundstock A, Liu Y, Huang A, Caro J. Amine-modified Mg-MOF-74/CPO-27-Mg membrane with enhanced H_2/CO_2 separation. Chemical Engineering Science. 2015;124:27-36.

[75] Herm ZR, Swisher JA, Smit B, Krishna R, Long JR. Metal−Organic Frameworks as Adsorbents for Hydrogen Purification and Precombustion Carbon Dioxide Capture. Journal of the American Chemical Society. 2011;133:5664-7.

[76] Herm ZR, Krishna R, Long JR. Reprint of: CO_2/CH_4, CH_4/H_2 and $CO_2/CH_4/H_2$ separations at high pressures using $Mg_2(dobdc)$. Microporous and Mesoporous Materials. 2012;157:94-100.

[77] Krishna R, van Baten JM. Investigating the potential of MgMOF-74 membranes for CO_2 capture. Journal of Membrane Science. 2011;377:249-60.

[78] Liu J, Benin AI, Furtado AMB, Jakubczak P, Willis RR, LeVan MD. Stability Effects on CO_2 Adsorption for the DOBDC Series of Metal–Organic Frameworks. Langmuir. 2011;27:11451-6.

[79] Lee D-J, Li Q, Kim H, Lee K. Preparation of Ni-MOF-74 membrane for CO_2 separation by layer-by-layer seeding technique. Microporous and Mesoporous Materials. 2012;163:169-77.

[80] Al-Naddaf Q, Thakkar H, Rezaei F. Novel Zeolite-5A@MOF-74 Composite Adsorbents with Core–Shell Structure for H2 Purification. ACS Applied Materials & Interfaces. 2018;10:29656-66.

[81] Banu A-M, Friedrich D, Brandani S, Düren T. A Multiscale Study of MOFs as Adsorbents in H_2 PSA Purification. Industrial & Engineering Chemistry Research. 2013;52:9946-57.

[82] Friebe S, Geppert B, Steinbach F, Caro J. Metal–Organic Framework UiO-66 Layer: A Highly Oriented Membrane with Good Selectivity and Hydrogen Permeance. ACS Applied Materials & Interfaces. 2017;9:12878-85.

[83] Huang K, Liu S, Li Q, Jin W. Preparation of novel metal-carboxylate system MOF membrane for gas separation. Separation and Purification Technology. 2013;119:94-101.

[84] Huang A, Chen Y, Liu Q, Wang N, Jiang J, Caro J. Synthesis of highly hydrophobic and permselective metal–organic framework $Zn(BDC)(TED)_{0.5}$ membranes for H_2/CO_2 separation. Journal of Membrane Science. 2014;454:126-32.

[85] Zhou S, Zou X, Sun F, Ren H, Liu J, Zhang F, et al. Development of hydrogen-selective CAU-1 MOF membranes for hydrogen purification by 'dual-metal-source' approach. International Journal of Hydrogen Energy. 2013;38:5338-47.

[86] Jin H, Wollbrink A, Yao R, Li Y, Caro J, Yang W. A novel CAU-10-H MOF membrane for hydrogen separation under hydrothermal conditions. Journal of Membrane Science. 2016;513:40-6.

[87] Park KS, Ni Z, Côté AP, Choi JY, Huang R, Uribe-Romo FJ, et al. Exceptional chemical and thermal stability of zeolitic imidazolate frameworks. 2006;103:10186-91.

[88] Novaković SB, Bogdanović GA, Heering C, Makhloufi G, Francuski D, Janiak C. Charge-Density Distribution and Electrostatic Flexibility of ZIF-8 Based on High-Resolution X-ray Diffraction Data and Periodic Calculations. Inorganic Chemistry. 2015;54:2660-70.

[89] Li W, Meng Q, Li X, Zhang C, Fan Z, Zhang G. Non-activation ZnO array as a buffering layer to fabricate strongly adhesive metal–organic framework/PVDF hollow fiber membranes. Chemical Communications. 2014;50:9711-3.

[90] Cacho-Bailo F, Catalán-Aguirre S, Etxeberría-Benavides M, Karvan O, Sebastian V, Téllez C, et al. Metal-organic framework membranes on the inner-side of a polymeric hollow fiber by microfluidic synthesis. Journal of Membrane Science. 2015;476:277-85.

[91] Li W, Zhang Y, Su P, Xu Z, Zhang G, Shen C, et al. Metal–organic framework channelled graphene composite membranes for H_2/CO_2 separation. Journal of Materials Chemistry A. 2016;4:18747-52.

[92] Bux H, Liang F, Li Y, Cravillon J, Wiebcke M, Caro J. Zeolitic Imidazolate Framework Membrane with Molecular Sieving Properties by Microwave-Assisted Solvothermal Synthesis. Journal of the American Chemical Society. 2009;131:16000-1.

[93] Xie Z, Yang J, Wang J, Bai J, Yin H, Yuan B, et al. Deposition of chemically modified α-Al_2O_3 particles for high performance ZIF-8 membrane on a macroporous tube. Chemical Communications. 2012;48:5977-9.

[94] Zhang S, Wang Z, Ren H, Zhang F, Jin J. Nanoporous film-mediated growth of ultrathin and continuous metal–organic framework membranes for high-performance hydrogen separation. Journal of Materials Chemistry A. 2017;5:1962-6.

[95] Hou J, Wei Y, Zhou S, Wang Y, Wang H. Highly efficient H_2/CO_2 separation via an ultrathin metal-organic framework membrane. Chemical Engineering Science. 2018;182:180-8.

[96] Li W, Shi J, Li Z, Wu W, Xia Y, Yu Y, et al. Hydrothermally Reduced Graphene Oxide Interfaces for Synthesizing High-Performance Metal–Organic Framework Hollow Fiber Membranes. Advanced Materials Interfaces. 2018;5:1800032.

[97] Kim S, Choi J, Choi C, Heo J, Kim DW, Lee JY, et al. Pore-Size-Tuned Graphene Oxide Frameworks as Ion-Selective and Protective Layers on Hydrocarbon Membranes for Vanadium Redox-Flow Batteries. Nano Letters. 2018;18:3962-8.

[98] Huang A, Liu Q, Wang N, Zhu Y, Caro J. Bicontinuous Zeolitic Imidazolate Framework ZIF-8@GO Membrane with Enhanced Hydrogen Selectivity. Journal of the American Chemical Society. 2014;136:14686-9.

[99] Zhang C, Xiao Y, Liu D, Yang Q, Zhong C. A hybrid zeolitic imidazolate framework membrane by mixed-linker synthesis for efficient CO_2 capture. Chemical Communications. 2013;49:600-2.

[100] Huang Y, Xiao Y, Huang H, Liu Z, Liu D, Yang Q, et al. Ionic liquid functionalized multi-walled carbon nanotubes/zeolitic imidazolate framework hybrid membranes for efficient H_2/CO_2 separation. Chemical Communications. 2015;51:17281-4.

[101] Huang A, Dou W, Caro J. Steam-Stable Zeolitic Imidazolate Framework ZIF-90 Membrane with Hydrogen Selectivity through Covalent Functionalization. Journal of the American Chemical Society. 2010;132:15562-4.

[102] Huang A, Caro J. Covalent Post-Functionalization of Zeolitic Imidazolate Framework ZIF-90 Membrane for Enhanced Hydrogen Selectivity. 2011;50:4979-82.

[103] Huang A, Wang N, Kong C, Caro J. Organosilica-Functionalized Zeolitic Imidazolate Framework ZIF-90 Membrane with High Gas-Separation Performance. 2012;51:10551-5.

[104] Brown AJ, Johnson JR, Lydon ME, Koros WJ, Jones CW, Nair S. Continuous Polycrystalline Zeolitic Imidazolate Framework-90 Membranes on Polymeric Hollow Fibers. 2012;51:10615-8.

[105] Huang A, Liu Q, Wang N, Caro J. Organosilica functionalized zeolitic imidazolate framework ZIF-90 membrane for CO_2/CH_4 separation. Microporous and Mesoporous Materials. 2014;192:18-22.

[106] Huang A, Bux H, Steinbach F, Caro J. Molecular-Sieve Membrane with Hydrogen Permselectivity: ZIF-22 in LTA Topology Prepared with 3-Aminopropyltriethoxysilane as Covalent Linker. 2010;49:4958-61.

[107] Knebel A, Wulfert-Holzmann P, Friebe S, Pavel J, Strauß I, Mundstock A, et al. Hierarchical Nanostructures of Metal-Organic Frameworks Applied in Gas Separating ZIF-8-on-ZIF-67 Membranes. 2018;24:5728-33.

[108] Dong X, Huang K, Liu S, Ren R, Jin W, Lin YS. Synthesis of zeolitic imidazolate framework-78 molecular-sieve membrane: defect formation and elimination. Journal of Materials Chemistry. 2012;22:19222-7.

[109] Cacho-Bailo F, Etxeberría-Benavides M, Karvan O, Téllez C, Coronas J. Sequential amine functionalization inducing structural transition in an aldehyde-containing zeolitic imidazolate framework: application to gas separation membranes. CrystEngComm. 2017;19:1545-54.

[110] Huang A, Chen Y, Wang N, Hu Z, Jiang J, Caro J. A highly permeable and selective zeolitic imidazolate framework ZIF-95 membrane for H_2/CO_2 separation. Chemical Communications. 2012;48:10981-3.

[111] Peng Y, Li Y, Ban Y, Jin H, Jiao W, Liu X, et al. Metal-organic framework nanosheets as building blocks for molecular sieving membranes. 2014;346:1356-9.

[112] Peng Y, Li Y, Ban Y, Yang W. Two-Dimensional Metal–Organic Framework Nanosheets for Membrane-Based Gas Separation. 2017;56:9757-61.

[113] Nian P, Liu H, Zhang X. Bottom-up fabrication of two-dimensional Co-based zeolitic imidazolate framework tubular membranes consisting of nanosheets by vapor phase

transformation of Co-based gel for H_2/CO_2 separation. Journal of Membrane Science. 2019;573:200-9.

[114] Xiang, Wu, ZhangZhang, Fu, Hu, ZhangZhang. A 3D Canted Antiferromagnetic Porous Metal−Organic Framework with Anatase Topology through Assembly of an Analogue of Polyoxometalate. Journal of the American Chemical Society. 2005;127:16352-3.

[115] Xiang S, He Y, Zhang Z, Wu H, Zhou W, Krishna R, et al. Microporous metal-organic framework with potential for carbon dioxide capture at ambient conditions. Nature Communications. 2012;3:954.

[116] Agueda VI, Delgado JA, Uguina MA, Brea P, Spjelkavik AI, Blom R, et al. Adsorption and diffusion of H_2, N_2, CO, CH_4 and CO_2 in UTSA-16 metal-organic framework extrudates. Chemical Engineering Science. 2015;124:159-69.

[117] Delgado JA, Águeda VI, Uguina MA, Brea P, Grande CA. Comparison and evaluation of agglomerated MOFs in biohydrogen purification by means of pressure swing adsorption (PSA). Chemical Engineering Journal. 2017;326:117-29.

[118] Brea P, Delgado JA, Águeda VI, Uguina MA. Comparison between MOF UTSA-16 and BPL activated carbon in hydrogen purification by PSA. Chemical Engineering Journal. 2019;355:279-89.

[119] Fu J, Das S, Xing G, Ben T, Valtchev V, Qiu S. Fabrication of COF-MOF Composite Membranes and Their Highly Selective Separation of H_2/CO_2. Journal of the American Chemical Society. 2016;138:7673-80.

[120] Das S, Ben T. A [COF-300]-[UiO-66] composite membrane with remarkably high permeability and H2/CO2 separation selectivity. Dalton Transactions. 2018;47:7206-12.

[121] Fischer M, Hoffmann F, Fröba M. Metal–organic frameworks and related materials for hydrogen purification: Interplay of pore size and pore wall polarity. RSC Advances. 2012;2:4382-96.

[122] Wu H, Yao K, Zhu Y, Li B, Shi Z, Krishna R, et al. Cu-TDPAT, an rht-Type Dual-Functional Metal–Organic Framework Offering Significant Potential for Use in H_2 and Natural Gas Purification Processes Operating at High Pressures. The Journal of Physical Chemistry C. 2012;116:16609-18.

[123] Yin H, Shang J, Choi J, Yip ACK. Generation and extraction of hydrogen from low-temperature water-gas-shift reaction by a ZIF-8-based membrane reactor. Microporous and Mesoporous Materials. 2019;280:347-56.

[124] Ranjan R, Tsapatsis M. Microporous Metal Organic Framework Membrane on Porous Support Using the Seeded Growth Method. Chemistry of Materials. 2009;21:4920-4.

[125] Takamizawa S, Takasaki Y, Miyake R. Single-Crystal Membrane for Anisotropic and Efficient Gas Permeation. Journal of the American Chemical Society. 2010;132:2862-3.

[126] Nandi S, De Luna P, Daff TD, Rother J, Liu M, Buchanan W, et al. A single-ligand ultra-microporous MOF for precombustion CO_2 capture and hydrogen purification. 2015;1:e1500421.

[127] Hu Y, Dong X, Nan J, Jin W, Ren X, Xu N, et al. Metal–organic framework membranes fabricated via reactive seeding. Chemical Communications. 2011;47:737-9.

[128] Zhang F, Zou X, Gao X, Fan S, Sun F, Ren H, et al. Hydrogen Selective NH_2-MIL-53(Al) MOF Membranes with High Permeability. 2012;22:3583-90.

[129] Guo H, Zhu G, Hewitt IJ, Qiu S. "Twin Copper Source" Growth of Metal−Organic Framework Membrane: $Cu_3(BTC)_2$ with High Permeability and Selectivity for Recycling H2. Journal of the American Chemical Society. 2009;131:1646-7.

[130] Nan J, Dong X, Wang W, Jin W, Xu N. Step-by-Step Seeding Procedure for Preparing HKUST-1 Membrane on Porous α-Alumina Support. Langmuir. 2011;27:4309-12.

[131] Mao Y, shi L, Huang H, Cao W, Li J, Sun L, et al. Room temperature synthesis of free-standing HKUST-1 membranes from copper hydroxide nanostrands for gas separation. Chemical Communications. 2013;49:5666-8.

[132] Nagaraju D, Bhagat DG, Banerjee R, Kharul UK. In situ growth of metal-organic frameworks on a porous ultrafiltration membrane for gas separation. Journal of Materials Chemistry A. 2013;1:8828-35.

[133] Mao Y, Li J, Cao W, Ying Y, Sun L, Peng X. Pressure-Assisted Synthesis of HKUST-1 Thin Film on Polymer Hollow Fiber at Room Temperature toward Gas Separation. ACS Applied Materials & Interfaces. 2014;6:4473-9.

[134] Li W, Meng Q, Zhang C, Zhang G. Metal–Organic Framework/PVDF Composite Membranes with High H_2 Permselectivity Synthesized by Ammoniation. 2015;21:7224-30.

[135] Hurrle S, Friebe S, Wohlgemuth J, Wöll C, Caro J, Heinke L. Sprayable, Large-Area Metal–Organic Framework Films and Membranes of Varying Thickness. 2017;23:2294-8.

[136] Li Y-S, Liang F-Y, Bux H, Feldhoff A, Yang W-S, Caro J. Molecular Sieve Membrane: Supported Metal–Organic Framework with High Hydrogen Selectivity. 2010;49:548-51.

[137] Li Y, Liang F, Bux H, Yang W, Caro J. Zeolitic imidazolate framework ZIF-7 based molecular sieve membrane for hydrogen separation. Journal of Membrane Science. 2010;354:48-54.

[138] Aceituno Melgar VM, Kwon HT, Kim J. Direct spraying approach for synthesis of ZIF-7 membranes by electrospray deposition. Journal of Membrane Science. 2014;459:190-6.

[139] Hillman F, Brito J, Jeong H-K. Rapid One-Pot Microwave Synthesis of Mixed-Linker Hybrid Zeolitic-Imidazolate Framework Membranes for Tunable Gas Separations. ACS Applied Materials & Interfaces. 2018;10:5586-93.

[140] Chang H, Wang Y, Xiang L, Liu D, Wang C, Pan Y. Improved H_2/CO_2 separation performance on mixed-linker ZIF-7 polycrystalline membranes. Chemical Engineering Science. 2018;192:85-93.

[141] McCarthy MC, Varela-Guerrero V, Barnett GV, Jeong H-K. Synthesis of Zeolitic Imidazolate Framework Films and Membranes with Controlled Microstructures. Langmuir. 2010;26:14636-41.

[142] Bux H, Feldhoff A, Cravillon J, Wiebcke M, Li Y-S, Caro J. Oriented Zeolitic Imidazolate Framework-8 Membrane with Sharp H_2/C_3H_8 Molecular Sieve Separation. Chemistry of Materials. 2011;23:2262-9.

[143] Yao J, Dong D, Li D, He L, Xu G, Wang H. Contra-diffusion synthesis of ZIF-8 films on a polymer substrate. Chemical Communications. 2011;47:2559-61.

[144] Pan Y, Wang B, Lai Z. Synthesis of ceramic hollow fiber supported zeolitic imidazolate framework-8 (ZIF-8) membranes with high hydrogen permeability. Journal of Membrane Science. 2012;421-422:292-8.

[145] Fan L, Xue M, Kang Z, Li H, Qiu S. Electrospinning technology applied in zeolitic imidazolate framework membrane synthesis. Journal of Materials Chemistry. 2012;22:25272-6.

[146] He M, Yao J, Li L, Zhong Z, Chen F, Wang H. Aqueous solution synthesis of ZIF-8 films on a porous nylon substrate by contra-diffusion method. Microporous and Mesoporous Materials. 2013;179:10-6.

[147] Huang K, Dong Z, Li Q, Jin W. Growth of a ZIF-8 membrane on the inner-surface of a ceramic hollow fiber via cycling precursors. Chemical Communications. 2013;49:10326-8.

[148] Zhang X, Liu Y, Kong L, Liu H, Qiu J, Han W, et al. A simple and scalable method for preparing low-defect ZIF-8 tubular membranes. Journal of Materials Chemistry A. 2013;1:10635-8.

[149] Shekhah O, Swaidan R, Belmabkhout Y, du Plessis M, Jacobs T, Barbour LJ, et al. The liquid phase epitaxy approach for the successful construction of ultra-thin and defect-free ZIF-

8 membranes: pure and mixed gas transport study. Chemical Communications. 2014;50:2089-92.

[150] Liu Y, Wang N, Pan JH, Steinbach F, Caro J. In Situ Synthesis of MOF Membranes on ZnAl-CO₃ LDH Buffer Layer-Modified Substrates. Journal of the American Chemical Society. 2014;136:14353-6.

[151] Zhang X, Liu Y, Li S, Kong L, Liu H, Li Y, et al. New Membrane Architecture with High Performance: ZIF-8 Membrane Supported on Vertically Aligned ZnO Nanorods for Gas Permeation and Separation. Chemistry of Materials. 2014;26:1975-81.

[152] Li J, Cao W, Mao Y, Ying Y, Sun L, Peng X. Zinc hydroxide nanostrands: unique precursors for synthesis of ZIF-8 thin membranes exhibiting high size-sieving ability for gas separation. CrystEngComm. 2014;16:9788-91.

[153] Su P, Li W, Zhang C, Meng Q, Shen C, Zhang G. Metal based gels as versatile precursors to synthesize stiff and integrated MOF/polymer composite membranes. Journal of Materials Chemistry A. 2015;3:20345-51.

[154] Drobek M, Bechelany M, Vallicari C, Abou Chaaya A, Charmette C, Salvador-Levehang C, et al. An innovative approach for the preparation of confined ZIF-8 membranes by conversion of ZnO ALD layers. Journal of Membrane Science. 2015;475:39-46.

[155] Liu Y, Peng Y, Wang N, Li Y, Pan JH, Yang W, et al. Significantly Enhanced Separation using ZIF‐8 Membranes by Partial Conversion of Calcined Layered Double Hydroxide Precursors. 2015;8:3582-6.

[156] Liu Y, Pan JH, Wang N, Steinbach F, Liu X, Caro J. Remarkably Enhanced Gas Separation by Partial Self-Conversion of a Laminated Membrane to Metal–Organic Frameworks. 2015;54:3028-32.

[157] Hu P, Yang Y, Mao Y, Li J, Cao W, Ying Y, et al. Room temperature synthesis of ZIF-8 membranes from seeds anchored in gelatin films for gas separation. CrystEngComm. 2015;17:1576-82.

[158] Hu Y, Wei J, Liang Y, Zhang H, Zhang X, Shen W, et al. Zeolitic Imidazolate Framework/Graphene Oxide Hybrid Nanosheets as Seeds for the Growth of Ultrathin Molecular Sieving Membranes. 2016;55:2048-52.

[159] Shamsaei E, Lin X, Wan L, Tong Y, Wang H. A one-dimensional material as a nano-scaffold and a pseudo-seed for facilitated growth of ultrathin, mechanically reinforced molecular sieving membranes. Chemical Communications. 2016;52:13764-7.

[160] Cacho-Bailo F, Caro G, Etxeberría-Benavides M, Karvan O, Téllez C, Coronas J. MOF–polymer enhanced compatibility: post-annealed zeolite imidazolate framework membranes inside polyimide hollow fibers. RSC Advances. 2016;6:5881-9.

[161] Hou J, Sutrisna PD, Zhang Y, Chen V. Formation of Ultrathin, Continuous Metal–Organic Framework Membranes on Flexible Polymer Substrates. 2016;55:3947-51.

[162] Chernikova V, Shekhah O, Eddaoudi M. Advanced Fabrication Method for the Preparation of MOF Thin Films: Liquid-Phase Epitaxy Approach Meets Spin Coating Method. ACS Applied Materials & Interfaces. 2016;8:20459-64.

[163] Wang X, Sun M, Meng B, Tan X, Liu J, Wang S, et al. Formation of continuous and highly permeable ZIF-8 membranes on porous alumina and zinc oxide hollow fibers. Chemical Communications. 2016;52:13448-51.

[164] Shamsaei E, Lin X, Low Z-X, Abbasi Z, Hu Y, Liu JZ, et al. Aqueous Phase Synthesis of ZIF-8 Membrane with Controllable Location on an Asymmetrically Porous Polymer Substrate. ACS Applied Materials & Interfaces. 2016;8:6236-44.

[165] Hu Y, Wu Y, Devendran C, Wei J, Liang Y, Matsukata M, et al. Preparation of nanoporous graphene oxide by nanocrystal-masked etching: toward a nacre-mimetic metal–organic framework molecular sieving membrane. Journal of Materials Chemistry A. 2017;5:16255-62.

[166] Li W, Su P, Li Z, Xu Z, Wang F, Ou H, et al. Ultrathin metal–organic framework membrane production by gel–vapour deposition. Nature Communications. 2017;8:406.

[167] He G, Dakhchoune M, Zhao J, Huang S, Agrawal KV. Electrophoretic Nuclei Assembly for Crystallization of High-Performance Membranes on Unmodified Supports. 2018;28:1707427.

[168] Cacho-Bailo F, Matito-Martos I, Perez-Carbajo J, Etxeberría-Benavides M, Karvan O, Sebastián V, et al. On the molecular mechanisms for the H_2/CO_2 separation performance of zeolite imidazolate framework two-layered membranes. Chemical Science. 2017;8:325-33.

[169] Kang Z, Fan L, Wang S, Sun D, Xue M, Qiu S. In situ confinement of free linkers within a stable MOF membrane for highly improved gas separation properties. CrystEngComm. 2017;19:1601-6.